Journal of South American Earth Sciences 80 (2017) 207–228

Contents lists available at ScienceDirect

Journal of South American Earth Sciences

journal homepage: www.elsevier.com/locate/jsames

U-Pb geochronology of Martín García, Sola, and Dos Hermanas Islands (Argentina and Uruguay): Unveiling Rhyacian, Statherian, Ectasian, and Stenian of a forgotten area of the Río de la Plata Craton

João O.S. Santos [a, *], Carlos J. Chernicoff [c, d], Eduardo O. Zappettini [d], Neal J. McNaughton [e], Y. Greau [b]

[a] Centre for Exploration Targeting, University of Western Australia, 35 Stirling Highway, Crawley, Perth, Western Australia, Australia
[b] Consejo Nacional de Investigaciones Científicas y Técnicas (CONICET), Argentina
[c] Servicio Geológico Minero Argentino (SEGEMAR), Argentina, Av. General Paz 5445 (colectora), Parque Tecnológico Miguelete, Edificio 25 San Martín (B1650 WAB), Provincia de Buenos Aires, Argentina
[d] John de Laeter Centre, Curtin University, Building 301, Bentley, Perth, Western Australia, Australia
[e] Centre for Geochemical Evolution and Metallogeny of Continents (GEMOC), Department of Earth and Planetary Sciences, Macquarie University, New South Wales, 2109 Sydney, Australia

ARTICLE INFO

Article history:
Received 1 September 2017
Accepted 24 September 2017
Available online 28 September 2017

Keywords:
Río de la Plata Craton
Martín García island
U-Pb zircon and titanite geochronology
Lu-Hf isotopes
Transplatense Orogen
Metacraton

ABSTRACT

The Río de la Plata Craton is one of the three major cratons of South America. The craton is largely covered by sedimentary basins where its most exposed area is Buenos Aires-Piedra Alta Province (Chernicoff et al., 2014). This province includes the Martín García Island in the confluence of Uruguay River and the Río de la Plata estuary. Despite to be a reference area for the craton the Martín García Island lacks modern geological investigation. We present U-Pb SIMS (secondary ion mass spectrometer) geochronological data on zircon and titanite, as well as Hf isotope determinations on zircon, from rocks of Martín García Island (Argentina), Sola and Dos Hermanas Islands (Uruguay) and from Paso Severino Formation (Uruguay). We investigated: 1) Rhyacian intermediate-to acidic plutonic, arc-type rocks of the Florida Belt dated between 2090 Ma and 2115 Ma, derived from juvenile Neoarchean crust (T_{DM}Hf: 2.52 Ga; average ε_{Hf}: +3.62); 2) Rhyacian metadacite (San José metamorphic belt) of 2127 Ma; 3) Statherian metagabbros of 1724–1734 Ma, with Transplatense inheritance; 4) Early Ectasian metagabbro of 1392 Ma, with Rhyacian inheritance; and 5) Stenian metagabbros of 1193 Ma (T_{DM}Hf: 2.00 Ga, ε_{Hf}: 0.1). Most of the dated orthogneisses show Brasilian-age (from 778 to 550 Ma) Pb loss in the zircons, interpreted to be caused by shearing or uplifting during Neoproterozoic. The results show that the area is not exclusively Rhyacian in age but encompasses Statherian, Ectasian, and Stenian gabbros. The last two are interpreted as distal intrusions associated to the Sunsás Orogen. All post-Transplatense metagabbros have geochemical signature of island arc basalt derived from primitive mantle with enrichment of LILE and depletion of HFSE. These characteristics point to the recurrence of magma chambers intermittently active during the Rhyacian, Statherian, Ectasian, and Stenian, all with a similar source. The term "Transplatense" is used to replace "Trans-Amazonian" events that occurred within the craton.

1. Introduction

The Río de la Plata Craton of southern South America (Fig. 1) encompasses autochthonous Precambrian Gondwana basement mostly covered (92%) by Paleozoic to Cainozoic sedimentary basins where the main cover is the Paraná Basin (Ordovician to Cretaceous). The concept of craton in South America (e.g. Almeida et al., 1976; Schobbenhaus and Neves, 2003) corresponds to crustal segments stable before the development of the Brasilian Orogen that is the pre-Neoproterozoic part of continental lithosphere. The craton is composed by different provinces/domains and one allochthonous terrane (Nico Pérez) – Fig. 1 - all formed from Paleoarchean to Mesoproterozoic; Santos et al., 2017).

* Corresponding author.
E-mail addresses: orestes.santos@bigpond.com (J.O.S. Santos), jorge.chernicoff@segemar.gov.ar (C.J. Chernicoff), eduardo.zappettini@segemar.gov.ar (E.O. Zappettini), N.McNaughton@curtin.edu.au (N.J. McNaughton), yoann.greau@mq.edu.au (Y. Greau).

https://doi.org/10.1016/j.jsames.2017.09.029
0895-9811/

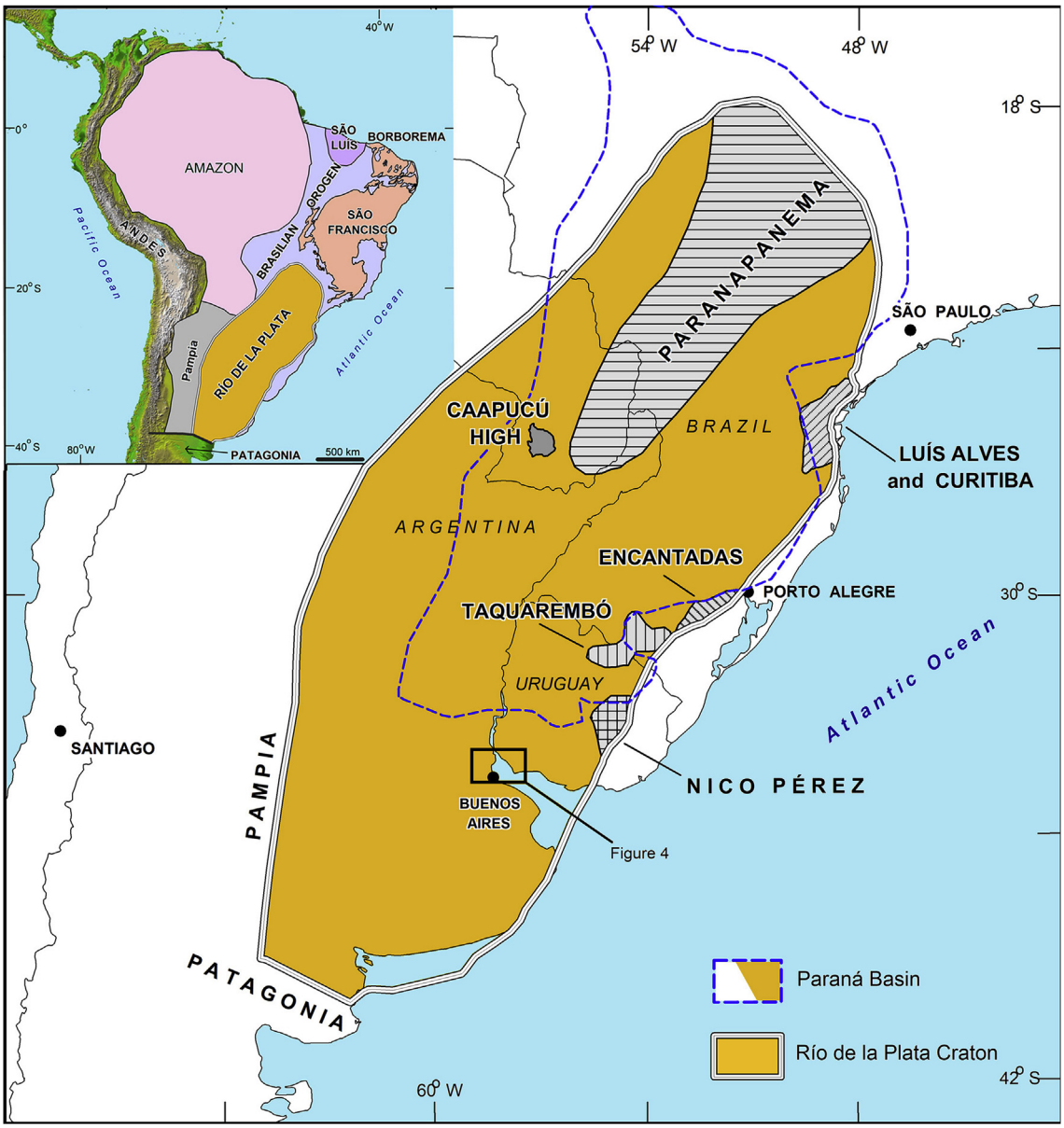

Fig. 1. Main geological components of Río de la Plata Craton. Inset shows the position in South America in relation to other four cratons. Outline of Paraná Basin (Ordovician to Cretaceous) also shown.

The geographic and temporal limits of the Río de la Plata Craton are poorly defined leading to eight different propositions (Rapela et al., 2007; Fuck et al., 2008; Bossi and Cingolani, 2009; Gaucher et al., 2009; Ramos et al., 2010; Oyhantçabal et al., 2011; Dragone et al., 2017; Fig. 3 of Santos et al., 2017). Parts of the craton are considered as other cratons or blocks, such as the Paranapanema (Fig. 1), Luís Alves, Curitiba, and Caapucú (Fig. 1). The timing of the craton is poorly defined. Some proposals consider that the craton is formed by only one province (the Buenos Aires-Piedra Alta, BAPA) comprising juvenile Rhyacian rocks (Rapela et al., 2011; Oyhantçabal et al., 2011; Oriolo et al., 2016). Other authors attribute a broader time span to the craton ranging from Archean to Stenian (e.g. Hartmann et al., 2001, 2008a, 2008b; Gaucher et al., 2011; Camozzatto et al., 2013; Chemale et al., 2011; Santos et al., 2017).

The largest province of the craton is the Buenos Aires-Piedra Alta which encompasses the Piedra Alta Complex of Uruguay (Florida, San José, and Arroyo Grande Belts) and the Buenos Aires Complex of Argentina Martín García, Tandilia Belt, and several occurrences under cover: city of Buenos Aires (Sociedad Rural and Riachuelo), Tapalqué well (Buenos Aires Province) - Chernicoff et al. (2016), and western Cordoba Province (Camilo Aldao and Ordoñez wells) (Rapela et al., 2007) (Fig. 2). A key area of the RLPC is the Martín García Island region in the northernmost exposed part of the Buenos Aires Complex. This reference area for the craton (Cingolani, 2011) only has K-Ar ages (1120–2085 Ma; Dalla Salda, 1981) are available for the island. Field work in the Martín García Island led to the recognition of new craton exposures in the two small islands located 15–20 km north along the Uruguay River.

The main exposed areas of the Río de la Plata Craton are along the Atlantic margin of the continent (Fig. 1), as in southern Brazil (Encantadas and Taquarembó domains – Hartmann et al., 2007;

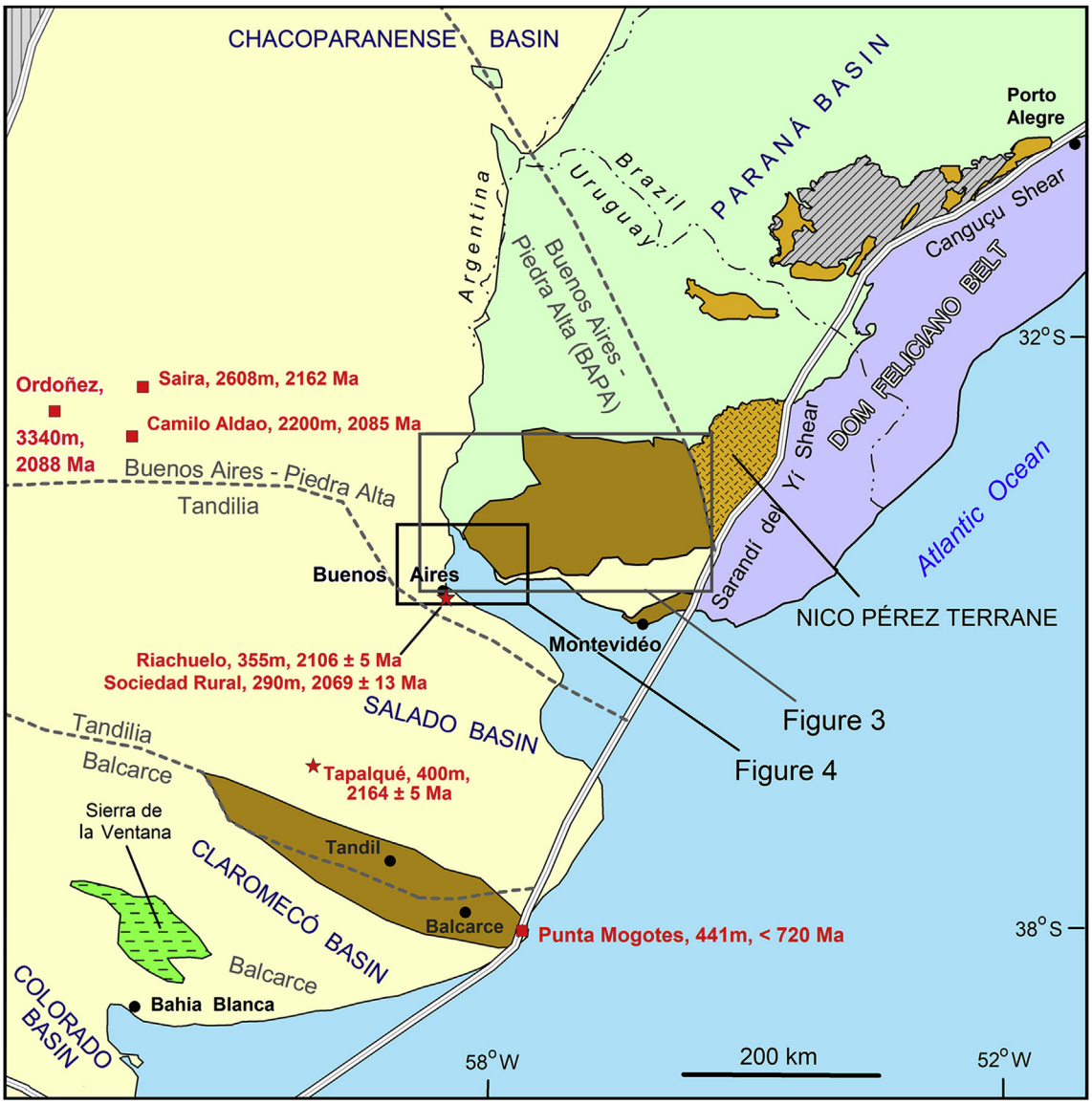

Fig. 2. Geological map of the southern part of the craton as adapted from Chernicoff et al. (2014) and Ramos et al. (2010) showing the exposed areas of the craton in ochre and light brown and the limits of the Buenos Aires-Piedra Alta, Tandilia, and Balcarce domains of the craton (grey dashed lines). The grey stripped area to the west-southwest of Porto Alegre in the metacratonic part of the craton. The location of seven dated drill cores is marked by quadrangles (Rapela et al., 2007; Punta Mogotes, Saira, Camilo Aldao, and Ordoñez) and stars (Chernicoff et al., 2015; Sociedad Rural, Richuelo, and Tapalqué). Rectangles indicate position of Fig. 3 and 4. (For interpretation of the references to colour in this figure legend, the reader is referred to the web version of this article.)

Curitiba and Luís Alves microcratons - Siga Jr. et al., 2007), Uruguay (Piedra Alta Province and Nico Pérez Terrane - Bossi et al., 1998; Hartmann et al., 2001), and also in the Buenos Aires Province of Argentina (Tandilia Belt; Cingolani, 2011; Cingolani et al., 2010). The Caapucú High in Paraguay (Fulfaro, 1996) is the northwesternmost exposition of the craton (Fig. 1). In addition, small outcrops of the craton occur within the Río de la Plata estuary, i.e. Martín García Island (Argentina), and small islands off the towns of Carmelo (Uruguay) and Colonia del Sacramento (Uruguay) - see Fig. 3. Seven samples from drill holes have provided access to the craton under cover (Rapela et al., 2011; Chernicoff et al., 2015), Fig. 2.

We present U-Pb SIMS (secondary ion mass spectrometer) geochronological data on zircon and titanite, as well as Hf isotope determinations on zircon, from basement rocks collected in the Martín García Island (Argentina), Sola and Dos Hermanas Islands (Uruguay) and from Paso Severino Formation (Uruguay).

1.1. The Río de la Plata Craton

The Rio de la Plata Craton is one of five cratons of South America. The second largest (about 2,400,000 km^2) after the Amazon craton of 6,000,000 km^2 (Santos et al., 2017). Approximately 92% of the RLP Craton is under cover – such as the Paraná Basin, Fig. 1 - making difficult the understanding of its extension and characterization of its domains and terranes. According to Santos et al. (2017) the craton is composed by several domains (and one terrane) (Table 1 and Fig. 1).

The eastern margin of the Río de la Plata Craton was strongly affected by the collisional orogenies of the Brasilian cycle leading to fragmentation and emplacement of Ediacaran magma within the

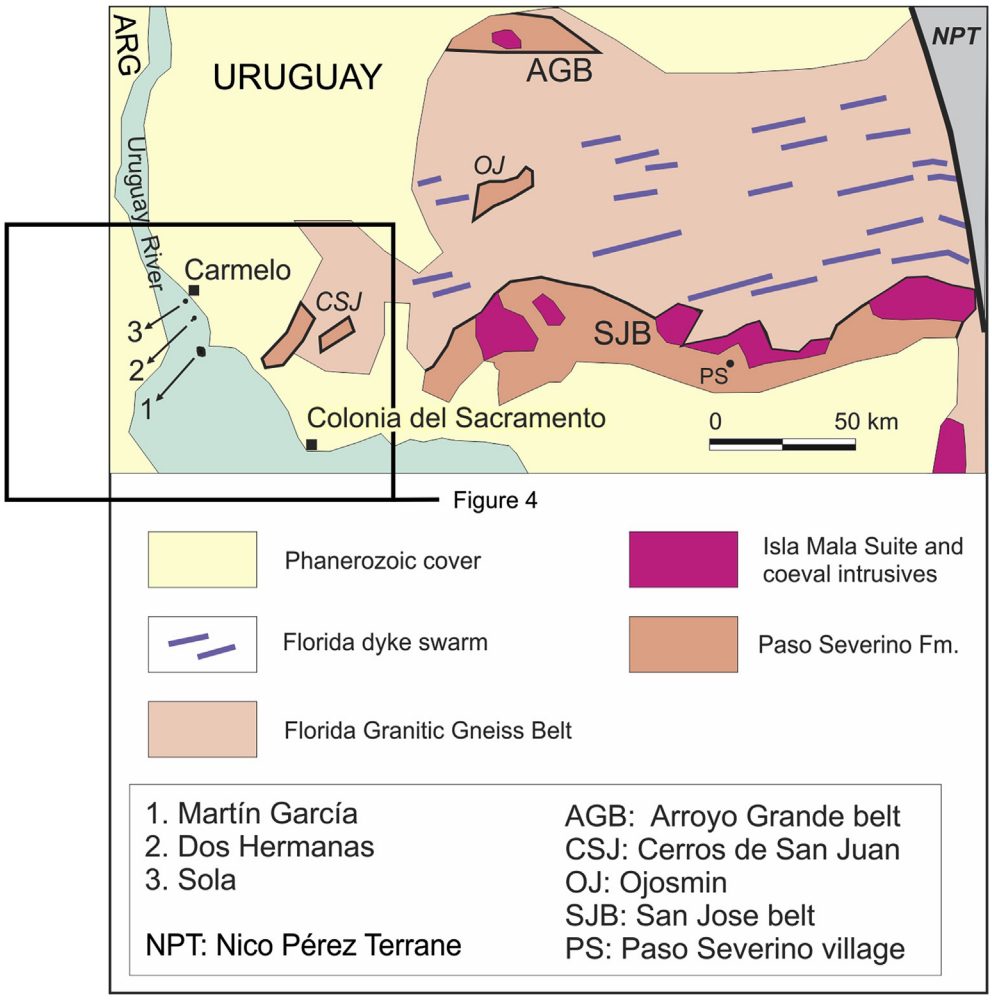

Fig. 3. Detail of Piedra Alta Complex in Uruguay including its belts: Florida (light salmon), Arroyo Grande (AG), San José (SJ), Ojosmin (OJ), Cerros de San Juan (CSJ). Location of the three investigated islands and Paso Severino village where sample A4 (metadacite) was collected.

Table 1
The main domains that make the Río de la Plata Craton.

Domain	Includes	U-Pb ages (Ma)	Main sources[a] (model-ages)
Luís Alves	Camboriú, Itapema	1560–2900	mature (2800–3400)
Curitiba	Atuba, Setuva	1850–3200	mature (2700–3100)
Caapucú	Tebicuary	1150–2050	undefined
Encantadas	Arroio dos Ratos	1580–2250	juvenile (1800–2250)
Taquarembó	Santa Maria Chico	1580–2350	mature (2550–3450)
Nico Perez terrane	Parque UTE, Illescas	1420–3450	juvenile and mature (2200–3700)
Buenos Aires-Piedra Alta	Tandilia	1180–2250	juvenile (2000–2400)

[a] Based on Hf, Nd data, and inherited U-Pb ages.

weakened zones of the craton. This process generated a tectonic mosaic of Rhyacian craton with Ediacaran pieces (orogenic). These characteristics constitute a metacraton (Liégeois et al., 2013) comparable to the 'metacratonic' nature of the Sahara Metacraton of Africa. In South America, the metacraton finds continuity in the Borborema Metacraton (Santos 2016). The area to the west of the Canguçu (Fernandes and Koester, 1999) and Sarandí del Yí (Bossi and Campal, 1992) shear system (Fig. 2) was considered metacraton by Santos et al. (2017).

1.2. Transplatense Orogen

The RLPC is dominated by Rhyacian units with traditional "Trans-Amazonian" age. The Trans-Amazon Orogen was defined as an orogenic cycle in northern South America by Hurley et al. (1967) using Rb-Sr and K-Ar ages of about 2000 Ma. We follow the recommendations of Neves et al. (2014) and Santos et al. (2017) and avoid using the term "Trans-Amazonian" outside the Amazon Craton and use "Transplatense" as proposed by Santos et al. (2017) to encompass the Rhyacian-age events that occurred within the Río

de la Plata Craton.

1.2.1. Buenos Aires-Piedra Alta (BAPA) Province

This province encompasses the Piedra Alta "terrane" (Bettucci et al., 2010) and the Buenos Aires "terrane" (Chernicoff et al., 2014). Piedra Alta includes the Florida, San José and Arroyo Grande Belts, and Buenos Aires includes the Tandilia Belt and the unexposed basement detected in several drill cores in the Cordoba and Buenos Aires Provinces. These two "terranes" are included in the Buenos Aires-Piedra Alta (BAPA) Province because they constitute a single tectono-stratigraphic unit formed by the Transplatense Orogen. The presence under cover of the Buenos Aires-Piedra Alta province is inferred from a gravimetric survey of Uruguay (Servicio Geográfico Militar del Uruguay, 1996).

The Buenos Aires Complex consists of gneiss, migmatite, amphibolite and minor ultramafic rocks, intruded by tonalitic/granitic and leuco-monzogranitic plutons. The complex is formed by arc-related granitoids of Rhyacian age (Rapela et al., 2011). There are also subordinate amounts of schist, marble, metavolcanic units, and dykes of felsic and mafic compositions. The Buenos Aires Complex is intruded by two unmetamorphosed dyke swarms: 1) A calc-alkaline swarm trending mainly E-W, dated by two ^{40}A-^{39}Ar step-heating plateau ages of plagioclase and biotite at 2020 ± 24 and 2007 ± 24 Ma (Teixeira et al., 2002), here interpreted as post-Transplatense minimum ages, and 2) A younger, Calymmian tholeiitic swarm trending WNW-ESE dated at 1588 ± 11 Ma (U-Pb on baddeleyite; Teixeira et al., 2002). The complex crops out in the three studied islands. Samples from the islands are considered part of the Buenos Aires Complex and Buenos Aires-Piedra Alta Province. Dalla Salda (1981) presented seven K-Ar ages for the Martín García Island (amphibole and muscovite, errors in the 50 Ma to 100 Ma range): three Rhyacian (2085, 2060, and 2050 Ma), two Orosirian (1870 and 1865 Ma), one Statherian (1600 Ma) and one Stenian (1120 Ma). Although minimum ages, they show the existence of Sunsás-age activity at about 1120 Ma and indicate that the island has more than one stratigraphic unit.

Zircon U-Pb SHRIMP ages for gneissic rocks and granitoids and charnockites of the Tandil area determined by Hartmann et al. (2002) and Cingolani et al. (2002, 2005) yielded Paleoproterozoic (Rhyacian) ages in the range of 2234–2065 Ma, with inheritances at 2368 Ma (Siderian), 2185 (Early Rhyacian) and 2657 Ma (Neoarchean). Hf and Nd isotopic data in the Tandil-Balcarce area (e.g. Hartmann et al., 2002; Pankhurst et al., 2003; Cingolani, 2011) indicate the hidden occurrence of Neoarchean crust in this segment of the Río de la Plata Craton.

The Buenos Aires-Piedra Alta Province is mostly exposed in southwestern Uruguay in large outcrops of granitic gneiss (Florida Granitic Belt), separated by two supracrustal metamorphic belts, i.e. the San José Belt in the southern part of the province, and the Arroyo Grande Belt in its northern part (e.g. Oyhantçabal et al., 2011). The Arroyo Grande Belt encompasses a folded greenschist facies volcano-sedimentary succession (depositional age estimated at ca. 2113 Ma; U-Pb conventional; Bossi and Ferrando, 2001). This succession was intruded by plutonic rocks dated at ca. 2076 Ma (U-Pb SHRIMP; Peel and Preciozzi, 2006). The San José Belt has amphibolite, paragneiss and micaschist (Montevideo and San José Formations; 2180-2120 Ma; Santos et al., 2003), and a meta-volcano-sedimentary succession (Paso Severino metadacite dated at 2146 ± 7 Ma; Santos et al., 2003). These successions were intruded by the calc-alkaline Isla Mala Suite (2074 ± 6 Ma and 2065 ± 9 Ma; Hartmann et al., 2000) and the late tectonic Rospide Gabbro, dated at 2075 ± 8 Ma (Hartmann et al., 2008a).

Post-orogenic plutons intruded into the Arroyo Grande and San José Belts are coeval with the gneisses and granites that make up the bulk of the central region extending in between the two belts, and are referred as Florida central gneiss belt (Oyhantçabal et al.,

Fig. 4. Satellite image of the Río de la Plata region between Argentina and Uruguay indicating the location of three studied islands. Detail of the sampling sites in Martín García Island in upper right inset. Also shown is San Gabriel Island (Uruguay), where Ribot et al. (2013) provided an age of 2040–2085 Ma for mylonite-granite.

2011). One exposure of the belt (San Gabriel Island) was studied by Ribot et al. (2013), a mylonite gneiss of 2078 ± 9 Ma (U-Pb LA-ICP-MS, zircon).

2. General sampling and exposures

The Martín García Island (Fig. 4) has a surface of ca. 4 km^2, roughly half of it is covered by alluvial sediments hence only ca. 2 km^2 represents craton. Nevertheless, Martín García Island encompasses a wide variety of rocks (Dalla Salda, 1981), predominant metagabbro, also metadacite – with metasedimentary xenoliths - as well as granodioritic, quartz-dioritic, syenogranitic, and trondhjemitic gneiss.

Sola Island has 0.12 km^2 and Dos Hermanas 0.24 km^2; most of their rocky shorelines are flooded in October–January. Consequently the exposed rocks and zircons are weathered and altered resulting in predominantly discordant ages.

Thirteen rock samples were collected for isotopic and geochemical analyses, corresponding to quartz-dioritic to granitic gneiss, metagabbro, felsic metavolcanic rock (metadacite). Eight of the analyzed rock types were collected at the Martín García Island, i.e. five occurrences of gabbro (MG200, MG202, MG204, MG205, and MG207), othogneiss (MG201 and MG206), and metadacite (MG203) – Fig. 4. All five analyzed rock samples collected at Sola and Dos Hermanas Islands (located in Figs. 3 and 4) are orthogneiss (IS1, IS2, 2H1, 2H2 and 2H3).

Most outcrops occur in the southern area of the Martín García Island as isolated exposures smaller than 100 m in length. The predominant rock type is metagabbro originally described as amphibolite by Dalla Salda (1981). On the whole, the Statherian metagabbros predominate, their weak sub-horizontal foliation and dark green color being distinctive. Microscopically, the samples are characterized by the predominance of plagioclase (calcic bytownite) with a large number of inclusions of small crystals of tremolite formed by metamorphism, minor pyroxene and olivine. The main normative composition of samples MG200-MG204 is 67–75% plagioclase, 14–23% hypersthene, 9–26% diopside, 4–9% olivine, 0.6–1.4% orthoclase, 0.34–1.46% ilmenite, and 0.74–1.25% magnetite (Table 2).

The younger metagabbro of Early Ectasian age (MG205) was sampled from an independent outcrop macroscopically not distinctive from the predominant Statherian olivine metagabbro. In this sample, metamorphic hornblende predominates over relict plagioclase (labradorite) largely altered to epidote. The normative composition of this metagabbro (MG205) is 53% plagioclase, 24% hypersthene, 13% diopside, 5% olivine, and 1.3% orthoclase.

Another low relief area near the coastline of Martín García Island included intermediate and felsic orthogneiss (MG206, quartz diorite, and MG201, granodiorite) and orthoschist (felsic volcanic protolith, MG203). This assemblage was cut by thin leucogranitic dykes and veins. Orthogneisses are medium-to coarse-grained, weakly banded, and have a uniform grey color. They include xenoliths of metasedimentary rock (not dated, assumed as Paso Severino Formation; see Discussion, below). Microscopically, these orthogneisses are characterized by mylonitic texture, including quartz ribbons, microcline, plagioclase (calcic oligoclase/andesine), aligned biotite, hornblende, and titanite. Their normative composition is: 17–28% quartz, 8.5–20.4% orthoclase, 41–58% plagioclase, 6–11% hypersthene. The dated orthoschist (MG203, metadacite), formed by quartz, plagioclase (oligoclase), microcline, tourmaline, hornblende and epidote.

The orthogneisses of the Sola and Dos Hermanas islands are massive to weakly foliated granitoids well exposed along the shoreline. Mylonitization mostly concentrates in narrow belts that alternate with less deformed rocks.

3. Methods

3.1. Geochemistry

Samples are analyzed for major elements by inductively coupled plasma (ICP-OES) and for trace and rare earth elements by ICP Mass Spectrometry (ICP-MS) at Activation Laboratories of Ancaster, Ontario, Canada. Actlabs has a routine practice where the entire rock is crushed to a nominal minus 10 mesh (1.7 mm), mechanically split to obtain a representative sample and then pulverized to at least 95% minus 200 mesh (−74 μm). All steel mills are mild steel and do not induce Cr or Ni contamination. Quality of crushing and pulverization is routinely checked as part of ActLabs quality assurance program. The most aggressive fusion technique employs a lithium metaborate/tetraborate fusion. Fusion is performed by a robot at Actlabs, which provides a fast fusion of the highest quality in the industry. The resulting molten bead is rapidly digested in a weak nitric acid solution. The fusion ensures that the entire sample is dissolved. It is only with this attack that major oxides including SiO_2, refractory minerals (i.e. zircon, sphene, monazite, chromite, gahnite, etc.), REE and other high field strength elements are put into solution. The analytical standards are NIST 694, DNC-1, GBW 07113, W-2a, SY-4, BIR-1a, and BCR-2. Representative data are presented in Table 2.

3.2. U-Pb analyses

Thirteen rocks were crushed, milled, sieved at 60 mesh, and washed to remove the clay and silt fractions. The remaining material, corresponding to fine sand and very fine sand, was dried and processed with one of two heavy liquids: LST (lithium-sodium tungstate, density 2.82 g/cm^3) and TBE (tetra-bromo-ethane, density 2.98 g/cm^3). The heavy mineral concentrates were separated into four fractions using a Frantz® magnetic separator. Using the lateral inclination of 5° and 1 A current zircon grains were picked from the less magnetic fraction and titanite from the more magnetic fraction. Grains were then mounted in epoxy discs of 2.5 cm diameter together with the analytical standards. The mounts were polished and coated with carbon for imaging using a TESCAN-VEGA3 Scanning Electron Microscope at the Centre for Microscopy, Characterization and Microanalyses of the University of Western Australia. This carbon coating was removed and replaced by gold coating for SIMS U-Pb analyses.

Sensitive High-mass Resolution Ion MicroProbe (SHRIMP II) U-Pb analyses of zircon and titanite were performed at Curtin University in four sessions using an analytical circular spot size of 20–25 μm in diameter. For several metamict grains spot size was 10–15 μm. About two minutes of rasterization was used to remove the gold coating which contains small amounts of common lead (ppb). Individual analyses are composed of nine measurements for zircon ($^{196}Zr_2O$, ^{204}Pb, background, ^{206}Pb, ^{207}Pb, ^{208}Pb, ^{238}U, ^{248}ThO, ^{254}UO), and nine measurements for titanite (^{200}Ti-Ca peak, ^{204}Pb, background, ^{206}Pb, ^{207}Pb, ^{208}Pb, ^{248}ThO, ^{254}UO, and $^{270}UO_2$) repeated in five scans. Zirocn standards D23 and glass NBS611 were used to identify the position of the mass peak ^{204}Pb, whereas the calibration of the U content and the Pb/U ratio used the zircon standard BR266 (559 Ma, 903 ppm U; Stern, 2001) and titanite standard Khan (522 Ma; 680 ppm U; Heaman, 2009). Data were reduced using SQUID© 2.50 software (Ludwig, 2009) and ages calculated using Isoplot© 3.0 (Ludwig, 2003). Most presented ages are upper intercept $^{207}Pb/^{206}Pb$ ages except for sample IS2, for which a concordia age was obtained from the concordant data. All ages were calculated at 2σ level and the individual analyses are quoted at 1σ level (Tables 3 and 4).

Table 2
Major and trace elements of samples from Martín García, Sola, and Dos Hermanas Islands.

Sample	IS1	IS2	2H1	2H2	2H3	MG200	MG201	MG202	MG203	MG204	MG205	MG206	MG207
Latitude	34.0225	34.0291	34.0700	34.0750	34.0791	34.1897	34.1902	34.1836	34.1841	34.1978	34.1849	34.1909	34.1761
Longitude	58.3033	58.3119	58.2808	58.2750	58.2725	58.2533	58.2533	58.2575	58.2524	58.2625	58.2554	58.2519	58.2472
rock	sgr	mgr	sgr	trd	sgr	omgb	grd	omgb	mdc	omgb	mgb	qzd	omgb
Major elements (%)													
SiO2	77.10	75.21	74.58	75.39	76.58	47.87	69.62	49.66	64.43	46.66	50.74	62.45	47.14
TiO2	0.093	0.095	0.167	0.123	0.076	0.178	0.384	0.155	0.767	0.149	0.176	0.568	0.206
Al2O3	12.24	13.62	12.39	12.1	12.8	22.18	13.59	17.81	16.11	24.77	16.5	16.89	14.87
Fe2O3(T)	1.78	1.41	2.32	1.87	1.44	5.08	2.78	5.55	4.99	4.68	6.70	4.82	7.85
MnO	0.048	0.028	0.031	0.041	0.024	0.085	0.033	0.111	0.058	0.072	0.122	0.07	0.129
MgO	0.12	0.18	0.07	0.15	0.08	6.70	1.05	9.89	1.57	5.71	11.43	2.04	12.95
CaO	0.62	1.12	0.74	0.93	0.68	14.58	2.63	13.49	4.53	14.38	10.35	4.88	13.81
Na2O	3.75	3.86	3.9	4.51	4.47	1.54	3.53	1.62	4.03	1.71	2.07	4.13	1.16
K2O	4.29	4.30	4.25	2.39	3.57	0.13	3.33	0.13	1.57	0.13	0.22	1.39	0.10
P2O5	<0.01	0.03	<0.01	<0.01	0.01	0.02	0.17	0.06	0.21	0.02	0.02	0.15	0.05
LOI	0.69	0.54	0.49	1.25	0.43	1.67	1.30	1.83	1.72	1.46	1.81	1.76	1.89
Total	100.7	100.4	98.95	98.77	100.2	100	98.41	100.3	99.99	99.75	100.1	99.14	100.2
Trace elements (ppm)													
Ag	2	1.9	5.5	1.9	1.6	<0.5	0.5	<0.5	0.6	<0.5	<0.5	<0.5	<0.5
As	<5	<5	<5	<5	<5	<5	9	<5	6	<5	<5	7	<5
Ba	357	480	2896	1389	238	281	921	510	518	57	95	355	43
Be	1	3	1	1	2	<1	2	<1	1	<1	<1	1	<1
Bi	<0.4	<0.4	<0.4	<0.4	<0.4	<0.4	<0.4	<0.4	<0.4	<0.4	<0.4	<0.4	<0.4
Ce	36.3	54.8	257	16.6	42.8	2.7	71.2	2.4	64.8	2.1	1	20.7	2.2
Co	6	5	5	3	5	34	32	38	34	30	39	26	54
Cr	80	120	90	40	130	580	30	430	<20	420	1040	30	1150
Cs	1.9	4.7	1	1.3	1.8	<0.5	1.2	<0.5	1.4	<0.5	<0.5	1.4	<0.5
Cu	<10	<10	<10	<10	<10	30	20	60	50	30	100	20	40
Dy	4.3	7.7	4.3	2	5.1	0.8	1.6	0.7	2.1	0.6	0.6	1.5	1
Er	2.5	5.6	2.4	1.2	3	0.5	0.9	0.4	1.1	0.4	0.4	0.8	0.6
Eu	0.31	0.44	1.21	0.26	0.25	0.33	0.72	0.29	1.07	0.33	0.28	0.77	0.3
Ga	19	20	18	17	18	11	15	10	17	12	9	17	8
Gd	4.4	5.6	5.8	1.8	5.3	0.7	2.3	0.7	2.9	0.5	0.5	1.8	0.8
Ge	2	2	2	2	2	1	1	2	1	1	2	<1	2
Hf	2.8	2.7	6.1	3.1	2.8	0.4	3.5	<0.2	4.2	<0.2	<0.2	3	<0.2
Ho	0.9	1.8	0.8	0.4	1	0.2	0.3	0.2	0.4	0.1	0.1	0.3	0.2
In	<0.2	<0.2	<0.2	<0.2	<0.2	<0.2	<0.2	<0.2	<0.2	<0.2	<0.2	<0.2	<0.2
La	16.1	27.4	138	9.7	19.5	1.2	36.1	1.6	31	0.9	0.5	12.4	1.4
Lu	0.36	0.95	0.39	0.25	0.42	0.07	0.11	0.06	0.15	0.05	0.06	0.11	0.08
Mo	<2	4	3	<2	4	<2	<2	<2	<2	<2	<2	<2	<2
Nb	6	16	6	5	7	<1	6	<1	7	<1	<1	5	<1
Nd	19.8	23.5	87.4	9.4	22.7	1.8	21.4	1.8	22.9	1.5	0.9	10.9	1.8
Ni	<20	<20	<20	<20	<20	130	<20	90	20	100	250	<20	210
Pb	14	31	11	10	14	<5	15	<5	6	<5	<5	7	<5
Pr	4.95	6.6	27.5	2.33	5.73	0.39	6.72	0.43	6.51	0.3	0.17	2.82	0.38
Rb	176	219	126	63	125	3	78	2	63	2	7	53	2
Sb	<0.5	<0.5	<0.5	<0.5	0.5	<0.5	<0.5	<0.5	<0.5	<0.5	<0.5	<0.5	<0.5
Sc	3	4	4	2	2	22	6	30	11	18	29	12	37
Sm	4.8	5.1	10.9	1.9	5.4	0.6	3.2	0.5	3.8	0.4	0.3	2.2	0.6
Sn	1	4	<1	1	1	<1	1	<1	2	<1	<1	3	<1
Sr	44	98	75	72	46	194	349	161	464	227	180	422	122
Ta	0.2	1.8	0.4	0.5	0.4	<0.1	1.1	<0.1	0.9	<0.1	<0.1	0.7	<0.1
Tb	0.7	1.1	0.8	0.3	0.9	0.1	0.3	0.1	0.4	0.1	<0.1	0.3	0.2
Th	3.8	21.9	14.1	11.4	17.4	<0.1	10.4	<0.1	6.8	<0.1	<0.1	2.8	<0.1
Tl	1	1.3	0.8	0.5	0.6	<0.1	0.4	<0.1	0.3	<0.1	<0.1	0.3	<0.1
Tm	0.38	0.86	0.35	0.2	0.47	0.08	0.12	0.07	0.15	0.06	0.06	0.12	0.09
U	1.5	4.2	1	1.9	4.2	<0.1	1.1	<0.1	0.9	<0.1	<0.1	0.6	<0.1
V	9	11	<5	9	<5	96	56	129	64	80	115	79	152
Y	23	57	20	13	33	5	8	6	11	4	4	9	6
Yb	2.3	5.8	2.2	1.4	3	0.5	0.8	0.4	1	0.4	0.4	0.7	0.6
Zn	40	50	60	50	<30	40	40	<30	50	<30	30	50	40
Zr	79	97	362	113	92	19	147	10	191	10	6	135	10
ΣREE	237.21	328.45	399.29	99.68	198.85	136.46	163.33	95.89	156.56	104.75	258.63	91.23	215.66
#Mg	13.01	22.12	6.29	15.13	11.03	74.58	45.63	79.88	41.16	73.08	79.14	48.51	78.59
Ca/(Ca + Na)	8.37	13.82	9.49	10.23	7.75	83.95	29.16	82.15	38.32	82.29	73.43	39.50	86.81
An-CIPW	8.37	13.40	6.88	10.23	7.62	79.35	25.83	73.68	36.74	79.49	65.35	38.52	77.10
CaO/Al2O3	0.05	0.08	0.06	0.08	0.05	0.66	0.19	0.76	0.28	0.58	0.63	0.29	0.93
La/Ta	80.50	15.22	345.00	19.40	48.75	N.A.	32.82	N.A.	34.44	N.A.	N.A.	17.71	N.A.
Ba/Ta	1785	267	7240	2778	595	N.A.	837	N.A.	576	N.A.	N.A.	507	N.A.
Ti/V	61.95	51.78	N.A.	81.93	N.A.	11.12	41.11	7.20	71.85	11.17	9.17	43.10	8.12
V/(Ti/1000)	16.14	19.31	N.A.	12.21	N.A.	89.96	24.33	138.83	13.92	89.56	108.99	23.20	123.08
Nd/Ce	0.55	0.43	0.34	0.57	0.53	0.67	0.30	0.75	0.35	0.71	0.90	0.53	0.82
La/Sm	3.35	5.37	12.66	5.11	3.61	2.00	11.28	3.20	8.16	2.25	1.67	5.64	2.33

(*continued on next page*)

Table 2 (*continued*)

Sample	IS1	IS2	2H1	2H2	2H3	MG200	MG201	MG202	MG203	MG204	MG205	MG206	MG207
Sm/Yb	2.09	0.88	4.95	1.36	1.80	1.20	4.00	1.25	3.80	1.00	0.75	3.14	1.00
Ti/Cr	6.97	4.75	11.12	18.43	3.50	1.84	76.74	2.16	0.00	2.13	1.01	113.51	1.07
Normative Minerals (%)													
Quartz	36.08	32.65	31.31	35.92	34.37	0	27.86	0	20.65	0	0	17.19	0
Plagioclase	34.81	38.02	35.59	42.78	41.13	66.15	40.91	54.43	55.11	73.96	52.56	58.18	44.89
Orthoclase	25.64	25.77	27.44	15.29	21.32	0.99	20.41	1.2	9.71	0.84	1.37	8.50	0.59
Corundum	0.25	0.58	0	0.19	0.33	0	0	0	0	0	0	0.02	0
Diopside	0	0	0.96	0	0	15.37	0.75	20.65	0.07	9.46	12.95	0	26.53
Hypersthene	2.70	2.28	2.64	2.83	2.08	9.3	5.51	15.6	9.60	3.52	24.22	10.92	7.24
Olivine	0	0	0	0	0	4.96	0	4.84	0	9.02	5.19	0	16.56
Ilmenite	0.17	0.19	0.32	0.23	0.15	0.34	0.72	0.3	1.46	0.28	0.34	1.08	0.4
Magnetite	0.29	0.23	0.38	0.3	0.23	0.81	0.45	0.88	0.8	0.74	1.07	0.77	1.25
Apatite	0	0.07	0	0	0.02	0.05	0.39	0.14	0.49	0.05	0.05	0.35	0.12
Total	99.94	99.79	98.64	97.54	99.63	97.97	97.00	98.04	97.89	97.87	97.75	97.01	97.58

Notes: * Rock acronyms: sgr = syenogranite; mgr = monzogranite; trd = trondhjemite; mgb = metagabbro; omgb = olivine metagabbro; mdc = metadacite; qzd = quartz diorite. N.A. = not available.

Table 3
Summary of dated rocks and determined U-Pb ages.

Sample	Rock	System/Period	Ages (Ma)	Lower intercept (Ma)	Inherited ages	Mineral	Figure
MG203	metadacite		2127 ± 6	550 ± 50		zircon and titanite	6a
IS1	syenogranitic gneiss		2115 ± 13	778 ± 74		zircon	6b
IS2	monzogranitic gneiss		2113 ± 10			titanite	6c
IS2			2098 ± 11			zircon	6c
MG206	quartz dioritic gneiss	Rhyacian	2103 ± 7	381 ± 36		zircon	6d
2H3	syenogranitic gneiss		2101 ± 13	661 ± 41		zircon	6e
MG201	granodioritic gneiss		2094 ± 9		2178 ± 8	zircon and titanite	6f
2H1	syenogranitic gneiss		2092 ± 13	651 ± 23		zircon	7a
2H2	trondhjemitic gneiss		2090 ± 10	604 ± 34	2732 ± 12	zircon	7b
MG200	olivine metagabbro	Statherian	1734 ± 20?		2105, 2116, 2439	zircon	Table 2
MG204	olivine metagabbro	Statherian	1724 ± 15		2035, 2601, 2934	zircon	7c
MG205	metagabbro	Early Ectasian	1392 ± 11	480 ± 90	2079 ± 36	zircon	7d
MG207	olivine metagabbro	Stenian	1187 ± 10		1250 ± 32	zircon	7e
MG202	olivine metagabbro	N.A.	N.D.				–

Location of samples (coordinates) are in Table 2.

3.3. Lu-Hf isotopes

Hf-isotope analyses were carried out using a New Wave/Merchantek UP213 laser-ablation microprobe, attached to a Nu Plasma multi-collector ICP-MS at GEMOC (Geochemical Evolution and Metallogeny of Continents), Macquarie University, Sydney. Operating conditions include a beam diameter of ±55 μm, a 5 Hz repetition rate, with energy of ~0.4–0.8 mJ. Typical ablation times are 100–120 s, resulting in pits 40–60 μm deep. Isobaric interference of ^{176}Yb on ^{176}Hf was corrected by measuring the interference-free ^{172}Yb isotope and then using the ^{176}Yb/^{172}Yb ratio to calculate the intensity of interference free ^{176}Yb. The appropriate value of ^{176}Yb/^{172}Yb was determined by analyzing the JMC475 Hf standard, which was successively doped with various amounts of Yb. Mud Tank (MT) zircon, which has an average ^{176}Hf/^{177}Hf ratio of 0.282522 ± 42 (2σ) (Woodhead and Hergt, 2005), was used as reference material to measure the accuracy of the results. MT analyzed in this study was within previously reported range (0.282531 ± 40; n = 14). The zircon standard Temora-2 was also run in order to monitor the efficiency of the Yb correction. The measured average ^{176}Hf/^{177}Hf of Temora-2 for this study is 0.282679 ± 19 (n = 3), which is within the range of previously reported values (0.282687 ± 24; Hawkesworth and Kemp, 2006). Temora-2 has typical ^{176}Yb/^{177}Hf ratios around 0.04, slightly higher than the average ^{176}Yb/^{177}Hf ratios of zircons in this study (0.034). More detail of the analytical techniques, precision and accuracy is described by Griffin et al. (2000, 2004).

Initial ^{176}Hf/^{177}Hf ratios are calculated using measured ^{176}Lu/^{177}Hf ratios, with a typical 2 standard error uncertainty on a single analysis of ^{176}Lu/^{177}Hf ± 1–2%. Such error reflects both analytical uncertainties and intragrain variation of Lu/Hf typically observed in zircons. The ^{176}Lu decay constant of Scherer et al. (2001) (1.865×10^{-11}) and the chondritic values of Blichert-Toft and Albarède (1997) are used for the calculation of ε_{Hf} values. Whilst a model of $(^{176}Hf/^{177}Hf)_i = 0.279718$ at 4.56 Ga and ^{176}Lu/^{177}Hf = 0.0384 has been used to calculate model ages (T_{DM}) based on a depleted-mantle source, producing a present-day value of ^{176}Hf/^{177}Hf (0.28325) (Griffin et al., 2000, 2004). T_{DM} ages, which are calculated using measured ^{176}Hf/^{177}Hf of the zircon, give only the minimum age for the source material from which the original magmas are derived. We have therefore also calculated a "crustal" model age (T^{C}_{DM}) for each zircon which assumes that the parental magma was produced from an average continental crust (^{176}Lu/^{177}Hf = 0.015; Griffin et al., 2004) that was originally derived from depleted mantle. The calculation of $\varepsilon_{Hf(t)}$ values was based on zircon SHRIMP U–Pb ages and the chondritic values of ^{176}Hf/^{177}Hf = 0.282772 and ^{176}Lu/^{177}Hf = 0.0332 (Scherer et al., 2001).

4. U-Pb geochronology

Thirteen samples were collected for U-Pb geochronology in:

Table 4
U-Pb-Th SHRIMP Data on zircon and titanite.

spot	U ppm	Th ppm	Th U	^{206}Pb ppm	4f^{206} %	isotopic ratios												ages						Disc. %
						^{207}Pb/^{206}Pb			^{207}Pb/^{235}U			^{206}Pb/^{238}U			Rho	^{208}Pb/^{232}Th			^{206}Pb/^{238}U			^{206}Pb/^{207}Pb			
2H1, syenogranitic gneiss, zircon																								
c.1-1	458	117	0.26	129.9	0.10	0.12560	±	0.46	5.7153	±	1.54	0.3300	±	1.47	0.955	0.0922	±	1.87	1839	±	23	2037	±	8	9.8
c.1-2	797	335	0.43	175.7	0.46	0.11671	±	0.67	4.1103	±	1.56	0.2554	±	1.41	0.903	0.0794	±	2.56	1466	±	18	1906	±	12	23.1
c.2-1	745	314	0.44	133.2	0.52	0.10680	±	0.72	3.0494	±	1.33	0.2071	±	1.12	0.841	0.0569	±	1.96	1213	±	12	1746	±	13	30.5
c.2-2	724	270	0.39	126.3	0.46	0.10613	±	0.82	2.9580	±	1.60	0.2021	±	1.37	0.858	0.0603	±	2.27	1187	±	15	1734	±	15	31.6
c.4-1	627	237	0.39	149.3	0.21	0.11983	±	0.49	4.5707	±	1.23	0.2766	±	1.13	0.918	0.0751	±	1.58	1574	±	16	1954	±	9	19.4
c.5.1	500	114	0.24	109.5	0.96	0.11979	±	1.28	4.1664	±	2.07	0.2523	±	1.62	0.785	0.0615	±	6.82	1450	±	21	1953	±	23	25.8
c.6-1	844	352	0.43	113.7	0.80	0.08948	±	1.32	1.9191	±	2.03	0.1555	±	1.54	0.761	0.0456	±	2.89	932	±	13	1415	±	25	34.1
c.6-2	606	181	0.31	140.1	0.22	0.11778	±	0.63	4.3627	±	1.71	0.2686	±	1.59	0.929	0.0711	±	2.41	1534	±	22	1923	±	11	20.2
c.7-1	933	386	0.43	130.2	0.81	0.09533	±	1.26	2.1182	±	1.98	0.1612	±	1.52	0.769	0.0441	±	3.14	963	±	14	1535	±	24	37.2
c.8-1	883	384	0.45	95.9	1.54	0.07512	±	2.10	1.2894	±	2.59	0.1245	±	1.53	0.588	0.0367	±	3.88	756	±	11	1072	±	42	29.4
c.2-1	793	303	0.39	229.3	0.14	0.12554	±	0.48	5.8145	±	1.15	0.3359	±	1.05	0.908	0.0953	±	1.43	1867	±	17	2036	±	9	8.3
c.7-1	743	287	0.40	255.2	0.02	0.13179	±	0.40	7.2641	±	1.15	0.3998	±	1.08	0.938	0.1118	±	1.29	2168	±	20	2122	±	7	−2.2
c.7-2	886	368	0.43	341.4	0.04	0.13254	±	0.36	8.1921	±	1.10	0.4483	±	1.04	0.944	0.1268	±	1.22	2388	±	21	2132	±	6	−12.0
2H2, trondhjemitic gneiss, zircon																								
e.3-1	1547	171	0.11	291.8	0.71	0.10492	±	0.74	3.1538	±	1.33	0.2180	±	1.11	0.833	0.0791	±	4.75	1271	±	13	1713	±	14	25.8
e.6-1	540	234	0.45	171.5	0.20	0.12894	±	0.44	6.5594	±	1.22	0.3690	±	1.14	0.932	0.0997	±	1.47	2025	±	20	2084	±	8	2.8
f.1-1	780	298	0.39	287.7	0.09	0.12870	±	0.60	7.6153	±	1.33	0.4292	±	1.18	0.893	0.1166	±	1.79	2302	±	23	2080	±	10	−10.7
f.2-1	106	41	0.40	47	0.15	0.18877	±	0.75	13.5055	±	1.78	0.5189	±	1.61	0.906	0.1350	±	2.46	2694	±	36	2732	±	12	1.7
f.6-2	395	148	0.39	125.1	0.15	0.12791	±	0.90	6.4895	±	1.68	0.3680	±	1.42	0.845	0.1001	±	2.22	2020	±	25	2069	±	16	2.4
f.8-1	939	82	0.09	494.2	0.29	0.13553	±	0.54	11.4110	±	1.26	0.6107	±	1.14	0.903	0.4916	±	2.23	3073	±	28	2171	±	9	−41.5
f.8-2	262	127	0.50	83.1	0.06	0.13098	±	1.06	6.6716	±	1.84	0.3694	±	1.51	0.819	0.1011	±	2.26	2027	±	26	2111	±	19	4.0
f.9-1	395	150	0.39	121.7	0.11	0.12953	±	0.91	6.4060	±	1.64	0.3587	±	1.36	0.832	0.0995	±	2.21	1976	±	23	2092	±	16	5.5
f.10-1	113	31	0.28	28.6	0.00	0.12338	±	1.86	5.0036	±	3.69	0.2941	±	3.18	0.863	0.0815	±	4.81	1662	±	47	2006	±	33	17.1
2H3 syenogranitic gneiss, zircon																								
b.2-2	5135	1562	0.31	904.7	0.18	0.09669	±	0.68	2.7294	±	1.30	0.2047	±	1.10	0.850	0.0573	±	1.55	1201	±	12	1561	±	13	23.1
b.1-1	2704	803	0.31	634.3	0.10	0.11956	±	0.50	4.4974	±	1.21	0.2728	±	1.10	0.910	0.0698	±	1.40	1555	±	15	1950	±	9	20.2
b.1-1B	4110	1127	0.28	700.8	0.19	0.10506	±	0.60	2.8692	±	1.26	0.1981	±	1.10	0.879	0.0568	±	1.72	1165	±	12	1715	±	11	32.1
b.2-1	461	118	0.26	129.3	0.21	0.12478	±	0.50	5.6020	±	1.51	0.3256	±	1.42	0.944	0.0881	±	2.11	1817	±	23	2026	±	9	10.3
b.2-2	804	338	0.43	171.7	0.80	0.11382	±	0.82	3.8702	±	1.63	0.2466	±	1.41	0.865	0.0726	±	2.89	1421	±	18	1861	±	15	23.7
b.2-3	731	273	0.39	125.5	0.46	0.10630	±	0.82	2.9178	±	1.63	0.1991	±	1.41	0.866	0.0596	±	2.28	1170	±	15	1737	±	15	32.6
e.1-1	1337	82	0.06	297	0.17	0.11904	±	0.37	4.2495	±	1.16	0.2589	±	1.10	0.946	0.2117	±	1.87	1484	±	15	1942	±	7	26.3
e.1-2	153	68	0.46	50	0.00	0.12856	±	0.70	6.7600	±	1.61	0.3814	±	1.45	0.900	0.1061	±	1.87	2083	±	26	2078	±	12	−0.2
e.2-1	375	119	0.33	120	0.06	0.12903	±	0.47	6.6203	±	1.32	0.3721	±	1.23	0.934	0.1030	±	1.61	2039	±	22	2085	±	8	2.5
e.8-1	334	78	0.24	106	0.09	0.12916	±	0.52	6.6038	±	1.81	0.3708	±	1.74	0.958	0.1058	±	2.24	2033	±	30	2087	±	9	3.0
IS1, syenogranitic gneiss, zircon																								
g.1-1	171	54	0.33	54.8	0.02	0.13003	±	0.67	6.6904	±	1.33	0.3732	±	1.15	0.864	0.1003	±	1.74	2044	±	20	2098	±	12	2.6
g.1-2	484	134	0.29	148.0	0.40	0.12820	±	0.67	6.2696	±	1.17	0.3547	±	0.95	0.817	0.1078	±	2.41	1957	±	16	2073	±	12	5.6
g.3-1	367	109	0.31	114.0	0.34	0.12780	±	0.67	6.3447	±	1.19	0.3601	±	0.98	0.826	0.0921	±	2.33	1983	±	17	2068	±	12	4.1
g.3-2	341	102	0.31	108.9	0.13	0.12881	±	0.56	6.5917	±	1.14	0.3711	±	0.99	0.870	0.1096	±	1.86	2035	±	17	2082	±	10	2.3
g.3-3	275	104	0.39	83.6	0.58	0.12869	±	1.01	6.2400	±	1.42	0.3517	±	1.01	0.707	0.1054	±	2.27	1943	±	17	2080	±	18	6.6
g.4-1	569	207	0.38	162.3	0.06	0.12616	±	0.40	5.7716	±	1.02	0.3318	±	0.94	0.919	0.0918	±	1.28	1847	±	15	2045	±	7	9.7
g.5-1	359	99	0.29	113.2	0.25	0.12906	±	0.56	6.5124	±	1.12	0.3660	±	0.97	0.867	0.1033	±	1.95	2010	±	17	2085	±	10	3.6
g.6-1	357	146	0.42	113.2	0.41	0.13046	±	0.64	6.6018	±	1.16	0.3670	±	0.97	0.837	0.1054	±	1.86	2015	±	17	2104	±	11	4.2
g.7-1	775	299	0.40	143.0	0.47	0.10446	±	0.71	3.0804	±	1.16	0.2139	±	0.92	0.793	0.0598	±	1.86	1249	±	10	1705	±	13	26.7
IS2, monzogranitic gneiss, titanite																								
a.2-1	321	59	0.19	88.0	0.60	0.13110	±	0.75	5.8056	±	1.46	0.3212	±	1.25	0.856	0.3110	±	0.45	1795	±	20	2113	±	13	17.2
a.2-2	207	87	0.43	65.0	0.70	0.13111	±	0.96	6.5874	±	1.66	0.3644	±	1.36	0.815	0.3599	±	0.51	2003	±	23	2113	±	17	6.0

(*continued on next page*)

Table 4 (*continued*)

spot	U ppm	Th ppm	Th U	^{206}Pb ppm	$4f^{206}$ %	isotopic ratios												ages						Disc. %
						$^{207}Pb/^{206}Pb$			$^{207}Pb/^{235}U$			$^{206}Pb/^{238}U$			Rho	$^{208}Pb/^{232}Th$			$^{206}Pb/^{238}U$			$^{206}Pb/^{207}Pb$			
a.3-1	104	50	0.49	27.5	0.54	0.13054	±	1.33	6.9880	±	2.70	0.3882	±	2.35	0.870	0.0594	±	3.65	2115	±	42	2105	±	23	−0.4
a.3-2	80	28	0.37	19.8	0.50	0.13030	±	1.38	6.9055	±	2.69	0.3844	±	2.31	0.858	0.0448	±	4.53	2097	±	41	2102	±	24	0.3
IS2, monzogranitic gneiss, zircon																									
h.1-1	103	37	0.37	25.6	0.47	0.12936	±	1.27	6.9240	±	2.62	0.3882	±	2.29	0.875	0.0452	±	4.06	2114	±	41	2089	±	22	−1.2
h.2-1	102	23	0.24	21.3	0.51	0.12919	±	1.46	6.8331	±	2.72	0.3836	±	2.29	0.844	0.0254	±	6.47	2093	±	41	2087	±	26	−0.3
MG200, olivine metagabbro, zircon																									
h.2-1	241	125	0.54	69.8	0.31	0.13131	±	0.67	6.0863	±	1.72	0.3360	±	1.59	0.921	0.0842	±	2.09	1868	±	26	2116	±	12	11.7
h.3-1	289	86	0.31	101.2	0.06	0.15847	±	0.49	8.9034	±	1.44	0.4075	±	1.35	0.939	0.1127	±	1.75	2203	±	25	2439	±	8	9.7
h.3-2	75	31	0.42	24.3	0.24	0.13051	±	1.20	6.7963	±	2.07	0.3777	±	1.70	0.817	0.0982	±	3.04	2065	±	30	2105	±	21	1.9
l.1-1	207	170	0.85	51.4	0.01	0.10613	±	1.07	4.2191	±	1.93	0.2883	±	1.61	0.833	0.0859	±	1.99	1633	±	23	1734	±	20	5.8
MG200, olivine metagabbro, rutile																									
i.1-1	4	1	0.21	N.D.	0.00	0.14420	±	3.49	N.D.	±	N.D.	N.D.	±	N.D.	N.D.	N.D.	±	N.D.	N.D.	±	N.D.	2278	±	60	N.D.
MG201, granodioritic gneiss, zircon																									
e.7-1	102	37	0.38	33.5	0.18	0.12888	±	1.37	6.7704	±	2.20	0.3810	±	1.72	0.782	0.1064	±	4.00	2081	±	31	2083	±	24	0.1
e.8-1	684	463	0.70	319.5	0.13	0.13606	±	0.46	10.1865	±	1.63	0.5430	±	1.57	0.960	0.1050	±	1.79	2796	±	36	2178	±	8	−28.4
e.9-1	196	51	0.27	65.4	0.11	0.12819	±	0.75	6.8474	±	1.72	0.3874	±	1.55	0.901	0.1048	±	5.12	2111	±	28	2073	±	13	−1.8
e.10-1	414	110	0.27	126.2	0.34	0.12997	±	0.92	6.3359	±	1.90	0.3535	±	1.67	0.876	0.0908	±	3.65	1952	±	28	2098	±	16	7.0
e.11-1	515	87	0.17	162.0	0.07	0.12956	±	0.65	6.5318	±	1.76	0.3657	±	1.63	0.928	0.1050	±	2.80	2009	±	28	2092	±	11	4.0
e.13-1	453	75	0.17	152.0	0.12	0.13103	±	0.72	7.0390	±	1.62	0.3896	±	1.45	0.897	0.1147	±	2.41	2121	±	26	2112	±	13	−0.4
MG201, granodioritic orthogneiss, titanite																									
e.1-2	100	102	1.05	33.5	2.64	0.12892	±	1.81	6.7123	±	2.14	0.3776	±	1.14	0.532	0.0974	±	2.95	2065	±	20	2083	±	32	0.9
e.1-2b	101	106	1.08	31.8	1.51	0.12974	±	1.28	6.4272	±	1.69	0.3593	±	1.11	0.654	0.0783	±	2.37	1979	±	19	2094	±	22	5.5
e.3-1	89	86	1.00	29.4	0.68	0.13069	±	1.19	6.8898	±	1.64	0.3823	±	1.12	0.686	0.1614	±	1.56	2087	±	20	2107	±	21	1.0
e.3-2	86	82	0.99	28.1	0.60	0.13153	±	0.99	6.8741	±	1.48	0.3790	±	1.10	0.745	0.1615	±	1.47	2072	±	20	2119	±	17	2.2
e.4-1	100	101	1.05	33.5	0.63	0.12963	±	0.72	6.9315	±	1.30	0.3878	±	1.09	0.832	0.0748	±	1.69	2113	±	20	2093	±	13	−0.9
e.4-2	109	112	1.06	36.3	0.83	0.12890	±	1.11	6.8173	±	1.56	0.3836	±	1.09	0.702	0.0939	±	1.89	2093	±	20	2083	±	19	−0.5
e.14-1	103	101	1.02	35.2	0.81	0.12945	±	1.03	7.0493	±	1.52	0.3949	±	1.11	0.731	0.2322	±	1.34	2146	±	20	2091	±	18	−2.6
MG203, metadacite, zircon																									
e.1-1	241	93	0.40	75.7	0.00	0.12986	±	0.87	6.5540	±	1.77	0.3660	±	1.54	0.871	0.1071	±	2.10	2011	±	27	2096	±	15	4.1
e.1-2-3	561	406	0.75	152.7	0.00	0.12653	±	0.69	5.5239	±	1.58	0.3166	±	1.43	0.901	0.0876	±	1.84	1773	±	22	2050	±	12	13.5
e.2-1	419	162	0.40	120.4	0.08	0.12912	±	0.95	5.9459	±	1.80	0.3340	±	1.53	0.849	0.0980	±	2.42	1858	±	25	2086	±	17	10.9
e.4-1	209	109	0.54	66.2	0.00	0.13093	±	1.00	6.6429	±	1.90	0.3680	±	1.61	0.848	0.1077	±	2.16	2020	±	28	2110	±	18	4.3
e.5-1	282	141	0.52	86.8	0.00	0.12990	±	0.77	6.4125	±	1.74	0.3580	±	1.55	0.896	0.0995	±	1.93	1973	±	26	2097	±	14	5.9
e.6-1	143	2	0.01	45.5	0.00	0.13083	±	1.09	6.6928	±	2.03	0.3710	±	1.72	0.843	0.1186	±	9.79	2034	±	30	2109	±	19	3.6
e.6-2-5	599	131	0.23	213.0	0.00	0.13328	±	0.57	7.6042	±	1.52	0.4138	±	1.40	0.926	0.1170	±	1.88	2232	±	27	2142	±	10	−4.2
e.8-1	342	95	0.29	93.8	−0.04	0.12781	±	0.63	5.6298	±	1.56	0.3195	±	1.43	0.915	0.0898	±	2.67	1787	±	22	2068	±	11	13.6
e.9-1	110	35	0.33	35.0	0.00	0.13141	±	0.85	6.7368	±	1.84	0.3718	±	1.64	0.889	0.1020	±	2.27	2038	±	29	2117	±	15	3.7
MG203, metadacite, titanite																									
e.6-1	71	72	1.05	22.4	0.74	0.12954	±	1.17	6.5389	±	1.84	0.3661	±	1.43	0.773	0.0748	±	2.25	2011	±	25	2092	±	21	3.9
e.6-2	47	47	1.04	15.5	0.96	0.13299	±	2.02	6.9704	±	2.65	0.3801	±	1.72	0.648	0.1131	±	2.84	2077	±	30	2138	±	35	2.9
e.7-1-2	32	30	0.99	10.7	1.30	0.13490	±	2.42	7.1625	±	2.89	0.3851	±	1.59	0.550	0.1508	±	2.76	2100	±	29	2163	±	42	2.9
e.7-2-3	61	60	1.02	19.4	0.66	0.13268	±	1.61	6.6832	±	2.17	0.3653	±	1.46	0.672	0.1665	±	2.01	2007	±	25	2134	±	28	5.9
MG204, olivine metagabbro, zircon																									
c.1-1-2	63	85	1.40	11.3	−0.09	0.10551	±	1.69	3.0337	±	2.62	0.2085	±	2.00	0.763	0.0630	±	3.80	1221	±	22	1723	±	31	29.1
c.1-2	153	79	0.54	19.2	0.48	0.12545	±	1.78	2.5207	±	2.34	0.1457	±	1.51	0.648	0.0581	±	2.95	877	±	12	2035	±	31	56.9
c.1-3	56	6	0.10	27.0	0.22	0.21374	±	0.96	16.6100	±	2.01	0.5636	±	1.77	0.878	0.1297	±	12.26	2882	±	41	2934	±	16	1.8
c.2-1	139	110	0.81	46.2	0.11	0.17445	±	0.73	9.2904	±	1.77	0.3863	±	1.62	0.912	0.0956	±	1.94	2105	±	29	2601	±	12	19.0

c.2-2	100	77	0.80	25.0	0.25	0.10587	±	1.43	4.2603	±	2.15	0.2919	±	1.61	0.748	0.0751	±	2.39	1651	±	23	1729	±	26	4.5
c.2-3	484	336	0.72	55.6	0.49	0.10521	±	1.23	1.9319	±	1.82	0.1332	±	1.34	0.737	0.0343	±	2.20	806	±	10	1718	±	23	53.1
MG205, metagabbro, zircon																									
b.1-2	88	87	0.99	18.2	0.10	0.08795	±	0.85	2.9238	±	1.41	0.2411	±	1.13	0.801	0.1107	±	1.42	1392	±	14	1381	±	16	−0.8
b.1-3	257	251	0.98	53.2	0.02	0.08883	±	0.66	2.9518	±	1.32	0.2410	±	1.14	0.865	0.1449	±	1.26	1392	±	14	1400	±	13	0.6
b.3-1	37	35	0.95	7.9	0.26	0.08919	±	2.11	3.0185	±	2.57	0.2454	±	1.46	0.570	0.2728	±	1.86	1415	±	19	1408	±	40	−0.5
b.3-2-3	64	61	0.95	12.8	0.27	0.08920	±	1.76	2.8586	±	2.12	0.2324	±	1.19	0.560	0.1498	±	1.63	1347	±	14	1408	±	34	4.3
b.3-3	86	84	0.98	16.8	0.22	0.08765	±	1.23	2.7371	±	1.67	0.2265	±	1.12	0.672	0.1206	±	1.43	1316	±	13	1375	±	24	4.3
b.4-1	41	42	1.02	14.0	1.71	0.12859	±	2.02	6.8692	±	2.34	0.3874	±	1.17	0.500	0.1349	±	2.30	2111	±	21	2079	±	36	−1.6
b.4-2	160	155	0.97	33.0	0.12	0.08773	±	0.93	2.9011	±	1.45	0.2398	±	1.12	0.768	0.1772	±	1.26	1386	±	14	1377	±	18	−0.7
b.5-1	28	27	0.96	5.6	0.17	0.08741	±	3.32	2.8513	±	3.57	0.2366	±	1.32	0.369	0.1223	±	2.34	1369	±	16	1369	±	64	0.0
MG206, quartz dioritic gneiss, zircon																									
a.6-1	679	267	0.41	151.0	0.04	0.12344	±	0.50	4.4024	±	0.74	0.2587	±	0.54	0.737	0.0733	±	2.05	1483	±	7	2007	±	9	26.1
a.7-1	382	80	0.22	114.4	0.02	0.12906	±	0.56	6.2087	±	0.88	0.3489	±	0.68	0.772	0.0863	±	3.27	1929	±	11	2085	±	10	7.5
a.8-1	404	254	0.65	89.2	0.31	0.12356	±	0.91	4.3634	±	1.14	0.2561	±	0.69	0.606	0.0411	±	2.40	1470	±	9	2008	±	16	26.8
a.9-1	414	129	0.32	109.8	0.00	0.12594	±	0.57	5.3572	±	0.88	0.3085	±	0.67	0.760	0.0856	±	1.24	1733	±	10	2042	±	10	15.1
a.9-2	404	125	0.32	111.2	0.05	0.12775	±	0.59	5.6391	±	0.90	0.3201	±	0.68	0.751	0.0864	±	1.44	1790	±	11	2067	±	10	13.4
a.12-1	253	67	0.27	79.3	0.06	0.13018	±	0.88	6.5594	±	1.32	0.3655	±	0.98	0.745	0.0992	±	2.60	2008	±	17	2100	±	15	4.4
a.11-1	279	78	0.29	89.3	0.02	0.12986	±	0.65	6.6746	±	1.03	0.3728	±	0.80	0.773	0.1008	±	1.69	2042	±	14	2096	±	11	2.6
a.11-2	335	101	0.31	106.2	0.06	0.12965	±	0.63	6.5945	±	0.97	0.3689	±	0.74	0.763	0.1027	±	1.55	2024	±	13	2093	±	11	3.3
MG207, olivine metagabbro, zircon																									
e.1-1	144	106	0.76	24.9	−0.13	0.07999	±	1.00	2.2244	±	1.50	0.2017	±	1.12	0.746	0.0615	±	1.52	1184	±	12	1197	±	20	1.0
e.1-2	180	124	0.71	31.7	0.42	0.07912	±	2.01	2.2249	±	2.44	0.2040	±	1.39	0.568	0.0571	±	2.50	1197	±	15	1175	±	40	−1.8
e.2-1	441	201	0.47	74.4	0.18	0.08038	±	1.05	2.1732	±	1.60	0.1961	±	1.21	0.755	0.0544	±	1.91	1154	±	13	1206	±	21	4.3
e.3-1	196	116	0.61	34.6	0.03	0.07996	±	0.96	2.2593	±	1.42	0.2049	±	1.04	0.734	0.0620	±	1.53	1202	±	11	1196	±	19	−0.5
e.3-2	352	170	0.50	60.7	0.10	0.07952	±	1.15	2.1970	±	1.72	0.2004	±	1.28	0.743	0.0583	±	1.97	1177	±	14	1185	±	23	0.6
e.5-1	1086	32	0.03	182.7	0.00	0.07913	±	0.66	2.1378	±	1.16	0.1960	±	0.95	0.819	0.0564	±	3.28	1154	±	10	1175	±	13	1.9
e.5-2-2	225	164	0.76	39.6	0.40	0.08221	±	1.64	2.3167	±	1.98	0.2044	±	1.10	0.558	0.0597	±	1.96	1199	±	12	1250	±	32	4.1
e.5-3	2128	519	0.25	353.5	0.01	0.07914	±	0.44	2.1102	±	1.18	0.1934	±	1.09	0.929	0.0522	±	2.73	1140	±	11	1176	±	9	3.1
e.6-1	172	121	0.72	28.8	0.05	0.07938	±	1.01	2.1315	±	1.51	0.1947	±	1.12	0.743	0.0563	±	1.55	1147	±	12	1182	±	20	2.9

Notes: Isotopic ratios errors in %.
All Pb in ratios are radiogenic component, all corrected for ^{204}Pb.
Disc. = discordance, as 100 - 100{t[^{206}Pb/^{238}U]/t[^{207}Pb/^{206}Pb]}.
4f206 = (common ^{206}Pb)/(total measured ^{206}Pb) based on measured ^{204}Pb.
Uncertainties are 1σ; N.D. = not determined. Rho = error correlation.

Martín García Island, Argentinean territory (MG200, MG201, MG202, MG203, MG204, MG205, MG206 and MG207), Sola Island, Uruguay (IS1 and IS2), and Dos Hermanas Island, Uruguay (2H1, 2H2 and 2H3) - (Table 3).

Analytical results are grouped into two major age groups, Transplatense (Rhyacian) and post-Transplatense (Statherian, Early Ectasian and Stenian), and presented for the Martín García, Sola, and Dos Hermanas Islands, each in chronological order from the oldest to the youngest samples, following the order of Table 3. This table shows a summary of the dated rocks, and indicates the dated minerals for each sample. The U–Pb isotopic data are presented in Table 4. Sample MG202 produced meaningless zircon and titanite whereas the other 12 samples are meaningful; in three of them both zircon and titanite (IS2, MG201, and MG203). Because both zircon and titanite are magmatic they crystallized close in time in the three samples. Zircon and titanite data were plotted and calculated together.

Five out of 82 analyses are reversely discordant (Table 4). Reverse discordance is explained by three mechanisms: addition of Pb, loss of U, and analytical problems. Williams et al. (1984) suggested that reverse discordance results from migration of radiogenic Pb between different regions within a zircon crystal, rather than U-loss. Mattinson et al. (1996, reprinted 2013) consider that reverse discordance is also produced by the removal of U from high-U zones of zircon by hydrothermal/metamorphic fluids or by chemical weathering. The residual zircon is enriched in low-U zones which contain excess radiogenic Pb and produce reverse discordance. The discordant grain of sample MG201 is 2178 Ma old and older than all other dated zircon and titanite grouped at the age of 2094 Ma. All other four reversely discordant analyses have ages which are within error with the other dated grains. They have similar $^{207}Pb/^{206}Pb$ ages when compared to the other analyses and plot in the same regression line. This indicates that the amount of ^{206}Pb and ^{207}Pb was not affected, which precludes the hypothesis of radiogenic lead introduction in the grains. Four zircons with reversely discordant ages are metamict and relatively U-rich (599–939 ppm). The interpretation is that the uranium was partially removed from the crystals by chemical weathering. This process affected the $^{206}Pb/^{238}U$ and $^{207}Pb/^{235}U$ ages but not the $^{207}Pb/^{206}Pb$ ages.

4.1. Transplatense

4.1.1. Martín García Island, sample MG203 (metadacite)

Thirteen crystals were analyzed (nine zircons and four titanites). Titanite is poor in U (average 53 ppm); areas with higher U were selected for analyses. The darker areas of Fig. 5a have <20 ppm U and were not analyzed. All zircons are highly metamict (Fig. 5b) leading to use of a smaller spot size of about 12–15 μm to avoid common lead-rich areas. Zircons are magmatic, zoned, with an average of 323 ppm U, and Th/U average of 0.38. Most of the grains suffered lead-loss generating discordant data. However, all zircon (n = 9) and titanite (n = 4) data (n = 13) align in the same regression intercepting the concordia line at 2127 ± 6 Ma (Fig. 6a). This is the magmatic age of the metadacite. The lower intercept of 550 ± 50 Ma suggests that an event of late Brasilian age caused lead-loss in zircon and titanite (Fig. 6a).

4.1.2. Sola Island, sample IS1 (syenogranitic gneiss)

This sample is zircon-rich; several thousand zircons were separated and about two hundreds were mounted in an epoxy disc. Zircons are short prisms (aspect ratio 1:1 to 1:3), 100–300 μm long, U-rich (q71 to 775 ppm), Th/U ratios from 0.29 to 0.48. Fewer fractures and inclusions are present compared to previous samples (MG series) but they are also metamict making difficult the selection of areas with less than 1% common lead using a spot size of 20–25 μm. The selection of the areas with less common lead is made observing the first 20 s of the first scan on each analysis. When the counts of ^{204}Pb are high (usually higher than 1 count per second) the analysis is aborted and the analytical beam is moved to another area or grain. To improve the analysis of non-metamict portions, some of the analyses used a smaller spot of ±15 μm. Results are moderately discordant (2.3%–9.7%) but one grain is more discordant (g.7-1; 27%). All nine analyses plot Pb/U ratios in the same line intercepting the concordia line at 2115 ± 13 Ma (MSWD = 2.8; Fig. 6b). This is interpreted as the age of the orthogneiss. The lower intercept at 778 Ma (Cryogenian) is evaluated in the discussion section.

4.1.3. Sola Island, sample IS2 (monzogranitic gneiss)

The sample is zircon-poor and rich in titanite. Three zircon grains were extracted and two were dated. They are 80–100 μm long and have 321 and 207 ppm U. Titanite grains are light brown to caramel fragments, 80–300 μm in size. Grains have low common lead (average 0.51%), U content of 97 ppm (average). All four analyses are concordant generating a concordia age of 2098 ± 6 Ma (Fig. 6c). The two zircons have similar age of 2113 ± 10 Ma (Fig. 6c) and all six analyses have a combined age of 2099 ± 10 Ma.

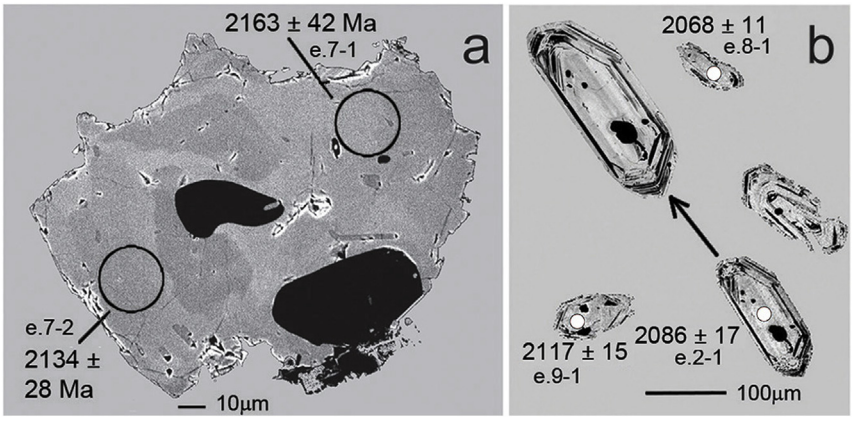

Fig. 5. Back-scattered electron images of titanite (a) and zircon (b) of MG203 metadacite. (a) - grain e.7 (titanite) showing two large inclusions, the location, and the ages of two spots. Darker areas are U-poor and were avoided. (b) Example of metamict zircon with scarce preserved areas.

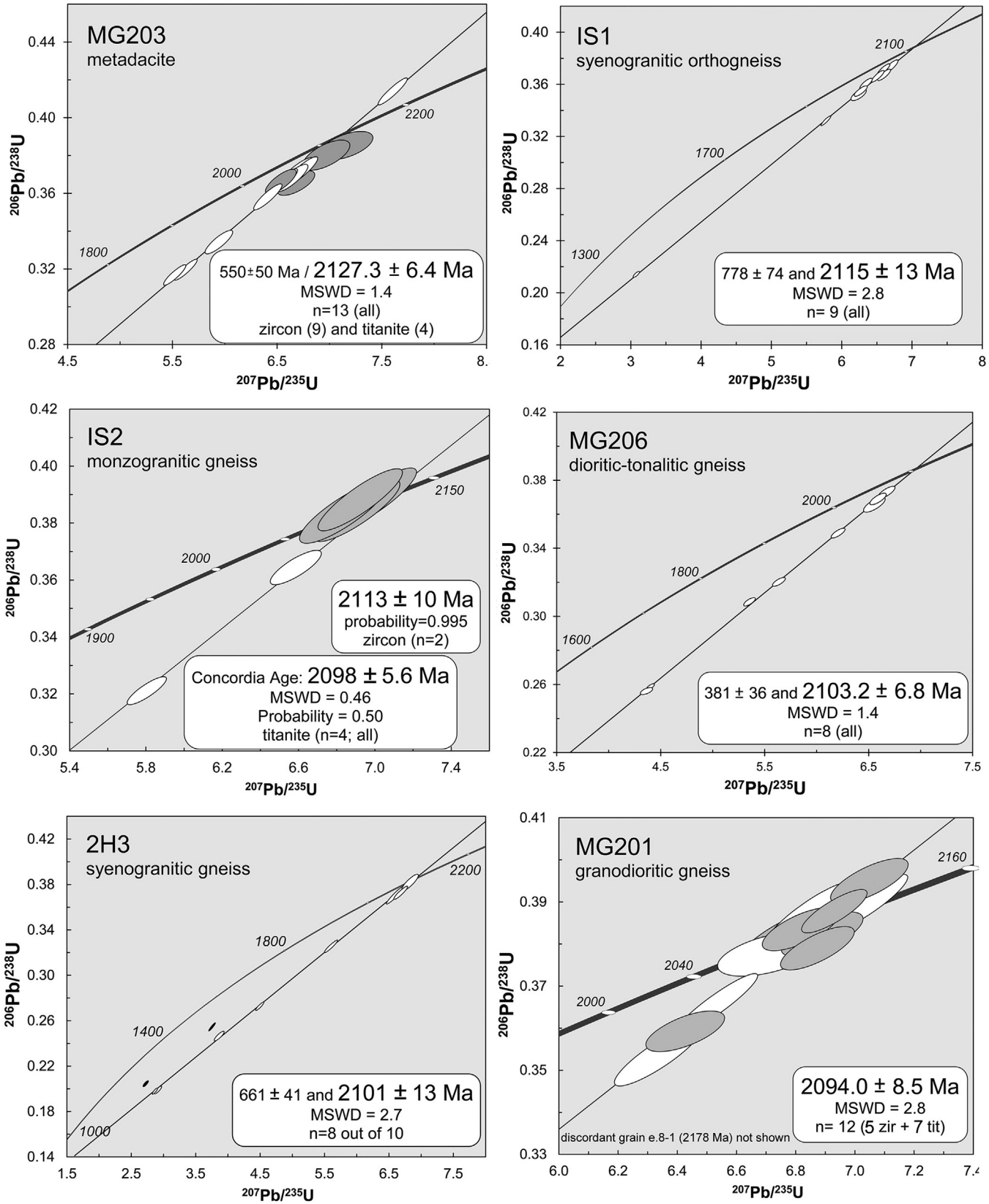

Fig. 6. Concordia diagrams: (a) Zircon (n = 9) and titanite (n = 4) data of MG203 metadacite showing regression line intercepting concordia at 2127 ± 6 Ma. Lower intercept is at 550 Ma. **(b)** Discordia line of zircons from syenogranitic gneiss (IS1) with the intercept age of 2115 ± 13 Ma (n = 9) and Cryogenian lower intercept age of 778 Ma. **(c)** Rhyacian zircon (2) and titanite (4) from monzogranitic gneiss IS2. Concordia age of titanite (n = 4) is 2098 ± 11 Ma whereas the mean average $^{207}Pb/^{206}Pb$ age of zircon and titanite data is 2099 ± 10 Ma. The age of two zircons (2113 ± 10 Ma) is within error of the titanite age. **(d)** Discordant data of zircon (n = 8) of quartz-dioritic gneiss (MG206) intercepting the concordia line at 2103 ± 7 Ma. **(e)** Discordia line of zircon (eight out of ten) of syenogranitic gneiss 2H3 determining an age of 2101 ± 13 Ma and another lower intercept of Brasilian age of 661 Ma. **(f)** Rhyacian zircon (n = 5) and titanite (n = 7) grains of granodioritic gneiss MG201 providing the age of 2094.0 ± 8.5 Ma (MSWD = 2.8). Inherited grain of 2178 Ma not shown.

4.1.4. Martín García Island, sample MG206 (quartz-diorite gneiss)

All zircons of this sample are highly metamict (U average = 394 ppm) but preserve prismatic shape and zonation. Most grains have excessively high common lead and only eight spots were analyzed. The data are discordant (from 2.6% to 26.8%) but all analyses follow a line intercepting the concordia curve at 2103 ± 7 Ma (MSWD = 1.4), which is considered the primary crystallization age of this orthogneiss. The imprecise lower intercept age of 381 ± 36 Ma finds no correlation to known thermal-tectonic events in the region (Fig. 6d).

4.1.5. Dos Hermanas island, sample 2H3 (syenogranitic gneiss)

A total of 10 zircon crystals were analyzed. Grains are short prisms (aspect ratio 1:1 to 1:2) with dark brown color, and are exceptionally rich in U (up to 5135 ppm; average 1614 ppm). All grains are partially to totally metamict requiring small analytical spot of 10 μm. The upper intercept in concordia is 2101 ± 13 Ma (MSWD = 2.7), which is interpreted as the age of this syenogranitic gneiss. The lower intercept (661 ± 41 Ma) reflects the age of radiogenic lead loss during the Brasilian Orogen, corresponding to the Cambaizinho orogeny (or complex) of South Brazil (Hartmann et al., 2011; Lena et al., 2014) - Fig. 6e.

4.1.6. Martín García Island, sample MG201 (granodioritic gneiss)

This sample produced more than 120 grains of low quality (dark, metamict, fractured), only 20 were mounted in epoxy. These zircons are darker and larger (150–300 μm long) than the zircons of samples MG203 and MG206. However, metamictization and presence of fractures and inclusions prohibit analysis; only six of them were analyzed. One grain is older, reversely discordant (28%) and inherited (e.8-1; 2178 ± 8 Ma). Titanite has light brown color forming equidimensional fragments of about 100–120 μm, internally homogeneous and free of inclusions and fractures. Seven analyses of titanite (Table 4) revealed reasonable content of U (average of 98 ppm) and relatively low common lead (average 1.1%). Pb/U ratios of 12 analyses (after removing the data of the inherited grain e.8-1) on five zircon and seven titanites are concordant (from −2.6% to 7% discordant) and follow discordia line of 2094 ± 8.5 Ma (MSWD = 2.8) - Fig. 6f.

4.1.7. Dos Hermanas island, sample 2H1 (syenogranitic gneiss)

Twelve zircon crystals were analyzed. Grains are short and dark prisms lacking pyramid terminations. They are U-rich (average 734 ppm) and metamict forcing using small analytical spot of 10–15 μm in two sessions. The data are up to 37% discordant including two reversely discordant analyses (see results and evaluation). However 12 out of 13 plot in the same regression line generating an upper intercept in the concordia line of 2092 ± 10 Ma (MSWD = 3.7, 2σ). This is considered the primary crystallization age of this syenogranitic gneiss, whereas the lower intercept (651 ± 23 Ma) reflects the age of an Brasilian-age Pb loss event (Fig. 7a). Such event is contemporaneous with one of the Brasilian orogenies such as the Cambaizinho (Lena et al., 2014; Hartmann et al., 2011).

4.1.8. Dos Hermanas island, sample 2H2 (trondhjemitic gneiss)

Eight zircon crystals were analyzed. Zircon is U-rich (up to 1547 ppm) and forms short prisms (aspect ratio 1:1 to 1:2) with well-defined pyramidal terminations. A grain with the least U (f.2-1; 106 ppm) is inherited, Archean in age (2732 ± 12 Ma). The other seven sub-concordant and discordant data form a discordia line intercepting the concordia curve at 2090 ± 10 Ma (MSWD = 1.5), and represents the primary crystallization age of this trondhjemitic gneiss. The lower intercept of 607 ± 34 Ma reflects the age of an Ediacaran Pb loss event temporally compared to the age of the Dom Feliciano orogeny of southern Brazil (Hartmann et al., 2003a) - Fig. 7b.

4.2. Statherian

4.2.1. Martín García Island, sample MG200 (olivine metagabbro)

This metagabbro is very poor in zircon and only few zircon grains were recovered from four samples. Four grains have ages of 1734, 2105, 2116, and 2479 Ma where 1734 ± 20 Ma (5.8% discordant) is the maximum age for the rock. The sample also has rutile and four grains were mounted to be analyzed. However, despite having no common lead the grains are extremely poor in U. One internal area in one grain has and 4 ppm U the resulting $^{207}Pb/^{206}Pb$ age is 2278 ± 60 Ma. Gabbroic rocks may contain inherited zircon and other U-carrying minerals. During the ascent of gabbroic magma the melt may incorporate or be contaminated by older host rocks. Most rocks are dissolved but zircon may survive to the process particularly when the gabbroic magma is or becomes saturated in Zr. This gabbro is an example of rock where all dated zircon and rutile are inherited which indicates that the rock is younger than 1734 Ma.

4.2.2. Martín García Island, sample MG204 (olivine metagabbro)

This gabbro produced few grains. Three analyses group at the age of 1724 ± 15 (Fig. 7c), similar to the youngest age of MG200 (1734 ± 20 Ma). The other three inherited zircons are Orosirian (2035 ± 31 Ma), Neoarchean (2601 ± 12 Ma), and Mesoarchean (2934 ± 16 Ma). The three Statherian grains (1718, 1723, and 1729 Ma) are rounded and have variable content of U (77–336 ppm) and Th/U ratios (0.72–1.40) and their ages are considered as inherited. The possible interpreted age is Mesoproterozoic just as as gabbros MG205 and MG207. Younger Neoproterozoic (Brasilian Orogen) or even Mesozoic age is not precluded, but less probable.

4.3. Ectasian

4.3.1. Martín García Island, sample MG205 (metagabbro)

This metagabbro has more zircon than MG200 and MG204. One grain is inherited (2079 ± 36 Ma) whereas the other seven group at the pooled age of 1392 ± 11 Ma (Ectasian) - Fig. 7d. All seven Ectasian zircons have similar Th/U ratios (from 0.95 to 1.02) and this is evidence that they crystallized from the same melt and are not inherited. This age is comparable to the age of 1375 ± 12 Ma of the Capivarita Anorthosite from the Encantadas Domain (Chemale et al., 2011) indicating that widespread mafic event occurred in the craton during Ectasian. The lower intercept of 480 ± 90 Ma suggests that an event of late Brasilian age caused lead-loss in the zircons. The only important known tectonic event occurring during the Early Ordovician-Late Cambrian Periods is the Búzios Orogeny (Schmitt et al., 2004) of eastern Brazil.

4.4. Stenian

4.4.1. Martín García Island, sample MG207 (olivine metagabbro)

Zircons from this metagabbro are prismatic, relatively large (150–600 μm) and displaying sharp (not rounded) edges. They are richer in U (average is 547 ppm) when compared to zircons from the other dated metagabbros and this richness is characteristic of magmatic zircon in gabbros (e.g. Williams and Hergt, 2000). The amount of common lead is low (average 0.12%). The concordia age of eight (out of nine) analyzed zircon grains yielded 1193 ± 8.1 Ma (MSWD = 1.2) - Fig. 7e. Because all grains have the same ages (within error), lack evidence of magmatic corrosion and are

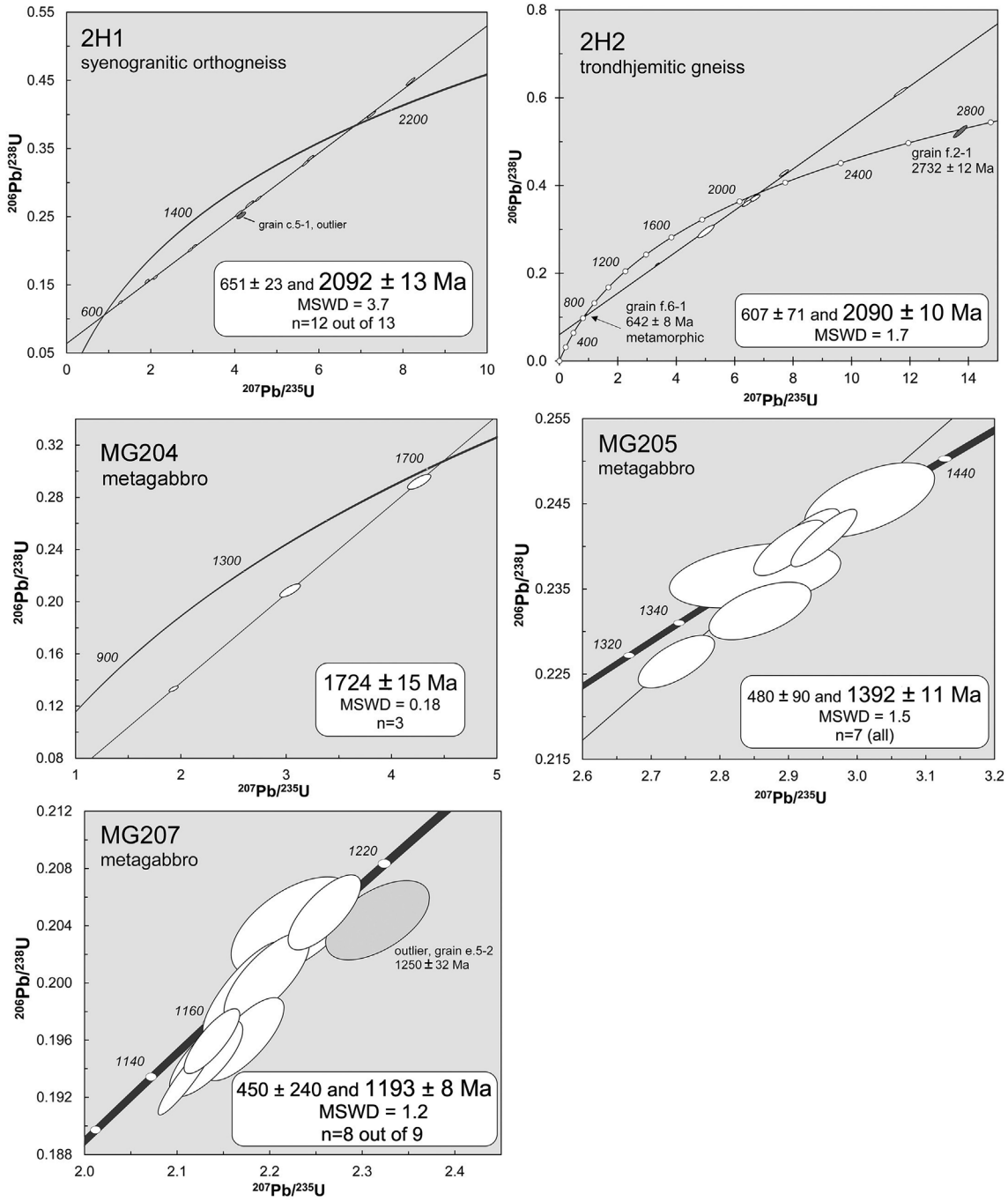

Fig. 7. Concordia diagrams: **(a)** Highly discordant data of zircon from sample 2H1 (syenogranitic gneiss) showing regression line intercepting concordia at 2092 ± 10 Ma and at 651 ± 23 Ma (n = 12 out of 13). **(b)** Discordia line for zircons of trondhjemitic gneiss 2H2 providing the age of 2092 ± 20 Ma. Lower intercept at 607 Ma indicates lead-loss during Brasilian times. Sample also has an inherited grain of 2732 Ma (not shown). **(c)** Statherian age (1724 ± 15 Ma) for three zircons of MG204 (olivine metagabbro). The rock has three inherited grains of 2035 ± 31 Ma, 2601 ± 12 Ma, and 2934 ± 16 (not shown). **(d)** Zircon data (n = 7) of MG205 metagabbro showing Ectasian age of 1392 ± 11 Ma and late Brasilian lower intercept at 480 ± 90 Ma. Inheritance at 2079 ± 36 Ma not shown. **(e)** Stenian zircon of olivine metagabbro MG207 providing the age of 1193 ± 10 Ma plus one inherited grain of 1250 Ma.

relatively rich in U, they are considered magmatic and not inherited.

5. Hf isotopes

Three samples were analyzed for Lu-Hf isotopes corresponding to one gabbro (MG207), one orthogneiss (MG201), and one metadacite (A4).

5.1. Sample MG201

Five measurements of Hf isotopes were undertaken on zircon from sample MG201 (granitic orthogneiss dated at 2094 ± 8.5 Ma) (Tables 3 and 4). All $^{176}Hf/^{177}Hf$ ratios of the measured zircon crystals are similar and the data have slightly positive values ε_{Hf} (average + 3.62). The average Lu-Hf model age of the zircon is 2.52 Ga (Fig. 8). This indicates that the Rhyacian granitic orthogneiss

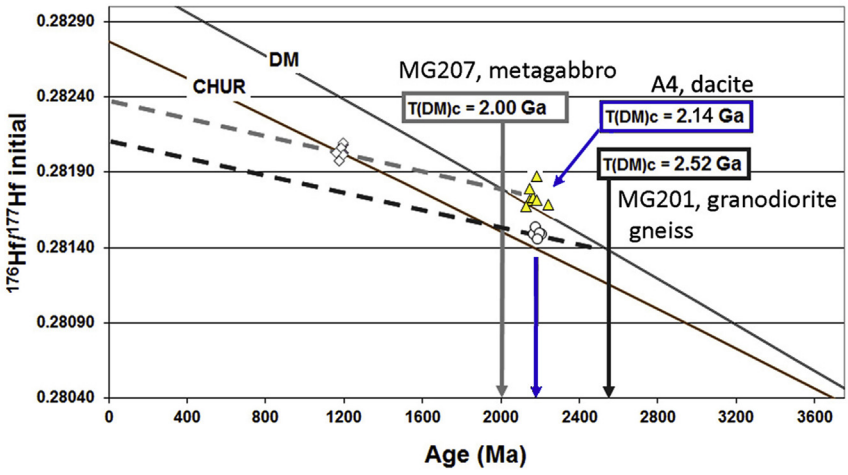

Fig. 8. Plot of $^{176}Hf/^{177}Hf$ ratios versus ages of five dated zircons of sample MG201 (granodioritic orthogneiss) and six zircons of sample MG207 (olivine metagabbro). The Depleted Mantle model-age (crustal) is Neoarchean (2.52 Ga) for the orthogneiss and Early Orosirian (2.00 Ga) for the gabbro. The slope of the dashed line uses the ratio of 0.015 for the $^{176}Lu/^{177}Hf$ ratio.

Table 5
Hf[a] composition of zircons from Martín Garcia Island and Paso Severino Formation.

	$^{207}Pb/^{206}Pb$ age (Ma)	$^{176}Yb/^{177}Hf$	$^{176}Lu/^{177}Hf$	$^{176}Hf/^{177}Hf$	error 1σ	ε_{Hf}	error 1σ	T^{C}_{DM} crustal
MG201, granodioritic gneiss								
e.7-1	2083	0.03172	0.000882	0.281521	0.000009	2.28	0.30	2.56
e.9-1	2073	0.03316	0.000994	0.281545	0.000014	2.90	0.49	2.51
e.10-1	2098	0.04538	0.001284	0.281565	0.000009	4.18	0.32	2.45
e.11-1	2092	0.03871	0.001086	0.281580	0.000020	4.57	0.70	2.42
e.13-1	2112	0.03147	0.000996	0.281556	0.000021	4.18	0.74	2.46
MG207, metagabbro								
e.1-1	1197	0.02464	0.000649	0.282083	0.000016	2.16	0.56	1.88
e.1-2	1175	0.03875	0.000887	0.282012	0.000011	−0.85	0.39	2.06
e.3-1	1196	0.02519	0.000630	0.282026	0.000009	0.09	0.30	2.01
e.3-2	1185	0.04201	0.001030	0.282060	0.000009	1.06	0.33	1.94
e.5-1	1175	0.03186	0.000894	0.281975	0.000008	−2.17	0.29	2.14
e.6-1	1182	0.02651	0.000637	0.282008	0.000010	−0.86	0.34	2.06
4A, dacite, Paso Severino Formation (U-Pb ages from Santos et al., 2003)								
a.1-1	2164	0.21293	0.005304	0.282065	0.000017	8.97	0.56	2.16
a.3-1	2111	0.09692	0.002760	0.281748	0.000022	9.95	0.49	2.11
a.4-1	2143	0.13131	0.003750	0.281851	0.000014	9.86	1.05	2.14
a.5-1	2165	0.17067	0.004820	0.281880	0.000030	11.65	0.74	1.99
a.7-1	2126	0.12790	0.003189	0.281886	0.000021	0.65	0.63	3.17
a.14-1	2125	0.11399	0.003009	0.281804	0.000016	10.04	0.60	2.17
a.15-1	2224	0.11505	0.002896	0.281771	0.000017	7.05	0.77	2.28

[a] ^{176}Lu decay constant $= 1.865 \times 10^{-11}$ (Scherer et al., 2001).

dated at ca. 2094 Ma was derived from juvenile Neoarchean crust.

5.2. Sample MG207

Six analyses of Hf isotopes were undertaken on zircons of sample MG207 (olivine metagabbro dated at 1193 ± 8 Ma) (Tables 3 and 4). All $^{176}Hf/^{177}Hf$ ratios of the measured zircons are similar and the data show slightly negative values ε_{Hf} (−0.1). The average Lu-Hf model age of the zircon is 2.00 Ga (Fig. 8). There was a small crustal contamination of a mantle-derived mafic melt with rocks much older than 2.00 Ga. Or else, the slightly negative ε_{Hf} value indicates that the mafic magma was derived from an enriched mantle barely contaminated by crustal components.

5.3. Sample 4A

All seven zircons of the Paso Severino metadacite (Table 5) have positive ε_{Hf} values. Grain 7-1 has a positive ε_{Hf} of 0.65, and the other six grains have highly positive values (average = 9.59). This is evidence of juvenile nature of Paso Severino volcanism (Fig. 8).

6. Geochemistry

6.1. Paleoproterozoic orthogneisses (quartz diorite-granite suite)

The SiO_2 contents range from 62.45 to 77.10% (Table 2). The distribution of TiO_2, $Fe_2O_{3(t)}$, CaO, MgO, Al_2O_3 and P_2O_5 show continuous and negative correlations with increasing SiO_2; whereas $NaO_2 + K_2O$ correlate positively with increasing SiO_2. According to their Na_2O and K_2O contents they are subalkaline.

Plotting data on A/CNK-A/NK diagram (Maniar and Piccoli, 1989; not shown) the samples have slightly peraluminous to metaluminous character. In the AFM diagram (Fig. 9a) the samples plot

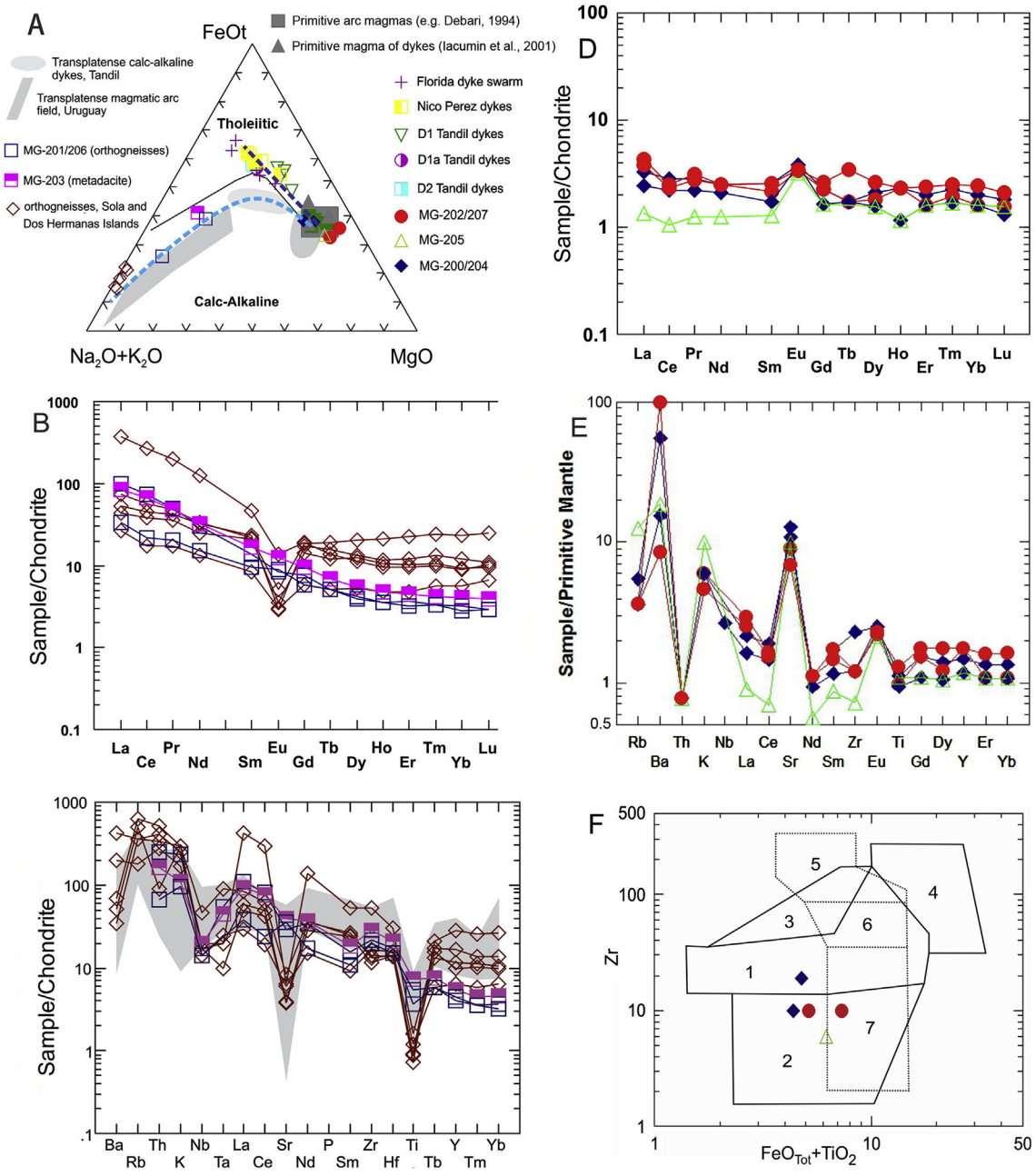

Fig. 9. (a) AFM plot for all the analyzed samples. Coeval lithologies from Tandilia and relevant Uruguayan rock units are plotted for comparison (after Iacumin et al., 2001; Bossi et al., 1996); (b) Chondrite–normalized REE (Sun and McDonough, 1989) patterns for the studied Paleoproterozoic rocks. References: open brown diamond (Sola and Dos Hermanas Islands orthogneisses; IS1, IS2, 2H1, 2H2, 2H3); dark blue open square (Martín García Island orthogneisses; MG201, MG206); magenta half solid square (Martín García Island metadacite; MG203); (c) Chondrite mantle-normalized spider diagrams (Thompson, 1982) for the studied Paleoproterozoic rocks. Grey area represents the range of the Transplatense magmatic arc. (d) Chondrite-normalized REE distribution patterns of Paleoproterozoic-Mesoproterozoic gabbros. (e) Primitive mantle normalized trace element distribution patterns of the gabbros. (f) Zr vs. FeO^{Tot} + TiO_2 diagram (tectonic classification of gabbros). Diagram after Biermanns (1996) where 1: N-type mid-ocean ridge (cumulate) + intracontinental rift (cumulate); 2: primitive mid-ocean ridge (cumulates); 3: N-type mid-ocean ridge (cumulate); 4: ocean island cumulate; 5: continental arc; 6: island-arc + continental arc; 7: island arc. Reference for symbols are in Fig. 9a. (For interpretation of the references to colour in this figure legend, the reader is referred to the web version of this article.)

within the calc-alkaline field. In accordance with the $(Na_2O + K_2O)$/CaO vs. Zr + Ce + Y + Nb diagram (Whalen et al., 1987) (not shown), they correspond to fractionated granite. Mesosilicic varieties plot in the medium-to high-K subseries (diagram after Gill, 1981; not shown).

The total REE varies from 91 to 399 ppm. Chondrite–normalized REE patterns display light rare earth element (LREE) enrichment and relatively flat patterns for the heavy rare earth elements (HREE), which suggest a shallow garnet-free source. Quartz dioritic to granodioritic rocks do not show Eu anomaly while granitic samples are characterized by having a sharp negative Eu anomaly related to plagioclase fractionation (Fig. 9b).

In a chondrite-normalized spider diagram (Fig. 9c) all samples exhibit enrichment in large–ion lithophile elements (LILE: Rb, K) relative to high–field–strength elements (HFSE: Nb, Ta, Ti), coincident with the Transplatense continental arc signature. The

negative Sr anomaly in the more siliceous samples is attributed to fractional crystallization in the magma source.

6.2. Paleoproterozoic to Mesoproterozoic gabbros

All gabbros show low concentrations (wt. %) of SiO_2 (46.66–50.74%), TiO_2 (0.155–0.206), Na_2O (1.16–2.07), K_2O (0.10–0.22) and high contents (with wide ranges) of Al_2O_3 (14.87–24.77), MgO (5.71–12.95), $Fe_2O_3^T$ (4.68–7.85) and CaO (10.35–14.58). High CaO and low SiO_2 are related to the presence of epidote. Low $Na_2O + K_2O$ is explained by the cumulate nature of the rocks. They are subalkaline and the CaO/Al_2O_3 ratios (0.58–0.93, average 0.71) are near to upper mantle ratio (0.8) (Sun and McDonough, 1989). Mg number varies between 73.08 and 79.88. The high Ni and Cr contents of these rocks vary between 90-250 ppm and 420–1150 ppm, respectively, suggest a tholeiitic origin.

Using the AFM diagram (Fig. 9a) the Paleoproterozoic to Mesoproterozoic gabbros are grouped in the field of primitive magmas (e.g. Debari, 1994, 1997), and are coincident with the primary magmas calculated by Iacumin et al. (2001) for Middle Proterozoic tholeiitic basaltic dykes of the Río de la Plata Craton.

The Ectasian gabbro (sample MG205) show high MgO (>8%), SiO_2 (>50%) and low TiO_2 (<0.4%), as well as unfractionated REE distribution pattern, that indicate a boninitic character with high CaO content. Chondrite normalized REE distribution patterns show no LREE enrichment, and flat HREE with positive Eu anomalies due to accumulation of plagioclase (Fig. 9d). Nd/Ce ratio (av. 0.77) is very close to the primitive mantle (0.76).

Primitive mantle normalized trace element distribution patterns show enrichment of LILE such as Rb, K, Sr and Ba, and depletion of HFSE such as Nb, Th and Hf. The pronounced positive spikes of Rb, Ba and K, and remarkable negative peaks of Nb and Th (Fig. 9e), produce high LILE/HSFE and LREE/HSFE ratios.

The geotectonic classification of the gabbros is made using Biermanns (1996) diagram using Zr vs. $FeO_{Tot} + TiO_2$. In this diagram (Fig. 9f), the Sthaterian and Stenian gabbros plot in the field of mid-ocean ridge (cumulate) gabbros. Using the TiO_2 - Y/20 - K_2O triangular diagram the Ectasian gabbro plots in the field of continental arc gabbro. Since this last unit has been affected by metamorphism the result is interpreted with care, due to low K_2O stability.

The Ti/Y ratios of gabbros are below 300, which indicate low Ti rocks. Incompatible trace element ratios such as La/Sm (3.2–1.67, av. 2.29; Primitive Mantle = 3.3) vs. Sm/Yb (1.25–0.75, average 1.04, Primitive Mantle = 0.9) are affected by the process of partial melting and the depth of melting. La/Sm is expected to be high when the degree of melting is low, and Sm/Yb is higher the deeper the depth of melting. The observed average high La/Sm values indicates that they result from a low to moderate degree of partial melting of upper mantle (spinel lherzolite). High Ba/La ratios (up to 320) are pointing to the presence of fluids in the source region during partial melting.

7. Discussion

The new data presented in this paper confirm the occurrence of both Transplatense and post-Transplatense rocks in the study area encompassing the Martín García (Argentina), Dos Hermanas, and Sola (Uruguay) Islands. These rocks are represented by intermediate-to acidic plutonic arc-type rocks and mafic plutonic extensional-type. In addition, the new data reveal the occurrence of units previously unknown in the study area, such as a felsic metavolcanic unit pertaining to the Transplatense magmatic arc, as well as Statherian, early Ectasian and Stenian gabbros.

7.1. Transplatense rocks of magmatic arc

The Transplatense rocks of magmatic arc exposed in the study area have ages between 2090 (2H2) and 2115 Ma (IS1). They are likely derived from rather juvenile Neoarchaean crust, as indicated e.g. by the Hf isotope composition – $T_{DM\text{-}Hf}$ 2.52 Ga and average ε_{Hf} values of +3.62 – of the zircons dated at 2094 Ma in a granitic orthogneiss (MG201). On a broader scale, these rocks are probably part of the westernmost Florida granitic-gneiss belt (e.g. Bossi et al., 1998), and are regarded as arc-related magmatic rocks (e.g. Bettucci et al., 2010). This orthogneiss may be the same tentatively dated by Dalla Salda (1981, K-Ar, amphibole) at 2085 ± 100, 2060 ± 100, and 2050 ± 100 Ma.

The U-Pb SIMS age obtained for the metadacite (MG203) is 2127.3 ± 6.4 Ma (plus Pb loss at 550 ± 50 Ma; see below) which suggests that this rock formed as part of the volcano-sedimentary Paso Severino Formation (San José Belt; Fig. 3), which occurs about 170 km to the east. This formation, in its type locality, is slightly older (i.e. metadacites dated at ca. 2146 ± 7 Ma with a lower intercept of 608 Ma; Santos et al., 2003). Additionally, undated metasedimentary xenoliths included in the orthogneiss MG201 (2094 ± 8.5 Ma; see Transplatense magmatic arc rocks, above) also point to the presence of the juvenile Paso Severino Formation in the study area. Accordingly, this evidence suggests that the San José metamorphic belt extends to the west at least up to the Martín García Island (see Fig. 3).

It is noticeable that the dated Transplatense granitoids are all affected by mylonitization (samples 2H1, 2H2 and 2H3) and show Pb loss of Brasilian age (lower intercept values at 651 Ma, 604 Ma and 661 Ma, respectively). The shearing and mylonitization are interpreted to be caused by the far field effect of Brasilian collisions, which are part of the overall effect of two of the five main Brasilian orogenies as defined by Hartmann et al. (2007, 2011). In accordance with the latter authors' terms, the 604–661 Ma Pb loss event falls within the Dom Feliciano and Passinho orogenies of the Brasilian Orogen. The concordia-discordia diagram of the felsic metavolcanic rock (sample MG203) also shows Ediacaran Pb loss at 550 ± 50 Ma.

Regionally, this effect is consistent with the pervasive hydrothermal event of Late Brasilian age (590–620 Ma) identified in the Tandilia region (Martínez et al., 2013; Angeletti et al., 2014, and references therein), and with the Pb loss of Brasilian age in rocks of Transplatense basement of southern Brazil-eastern Uruguay (e.g. Hartmann et al., 2003a,b).

In some cases, the Transplatense granitoids reveal a Cryogenian Pb loss event (e.g. sample IS-1) at ca 778 Ma, which is attributed to the thermal effect of the Cambaizinho orogeny of the Brasilian Orogen (Hartmann et al., 2011).

7.2. Statherian, Early Ectasian and Stenian gabbros

7.2.1. Statherian magmatism

In addition to the well-known Statherian mafic dyke swarm positioned parallel to the older fabric of the Buenos Aires-Piedra Alta province, we identified gabbros that are likely associated or linked with the conspicuous coeval mafic dykes pertaining to the diachronous extensional event initiated after the Transplatense Orogen, e.g. 1.73 Ga Florida tholeiitic dyke swarm of Uruguay and lasting up to ca. 1.59 Ga in the Tandilia Province (e.g. Mazzucchelli et al., 1995; Iacumin et al., 2001).

The newly dated gabbros yielded 1724 Ma (MG204) and 1734 Ma (MG200), with inheritance at 2035, 2601 and 2934 Ma (MG204) and at 2278 and 2479 Ma (MG200), pointing to both late Transplatense and older crust (Mesoarchean to Siderian). We interpret this inheritance as derived from the Transplatense magmatic arc and its (unexposed) Mesoarchean to Siderian basement.

In addition to the mafic dyke swarm and gabbros referred to above, the occurrence of metatuffs dated at ca. 1753 Ma at the nearby Cerros de San Juan (Peel and Preciozzi, 2006) is regarded by these authors as forming part of the San José metamorphic belt. This suggests that the Statherian magmatism in the Buenos Aires-Piedra Alta province is bimodal, consistently with its extensional setting. The metatuffs of Cerros de San Juan contain inherited zircons dated at 2358 Ma (Peel and Preciozzi, 2006), likely derived from the hidden Siderian basement. The unexposed occurrence of Siderian (as well as pre-Siderian) crust was included by Chernicoff et al. (2014) in their proposed early crustal evolution model of the southwestern Río de la Plata Craton.

We note a similarity between the key geochemical signatures of the Statherian gabbros and the coeval dykes (e.g. Mazzucchelli et al., 1995). However, the slightly enriched LREE and positive Eu anomaly of the analyzed gabbros indicate a signature of magmatic arc inherited from the Transplatense magmatism.

A space and time relationship between the tholeiitic, Statherian dyke swarm of the Buenos Aires-Piedra Alta Province (Florida or Uruguayan dyke swarm) and a coeval, causative mantle plume has been proposed by several authors, e.g. Halls et al. (2001). The IAVCEI's (International Association of Volcanology and Chemistry of the Earth's Interior) LIP (Large Igneous Provinces) commission regards the Uruguayan dyke swarm as representing a large igneous province – LIP N^{o} 137; 2000 km^2; rated as "B5"– considered to be linked to a mantle plume head (see e.g. Ernst, 2014, and references therein). In contrast to the latter view, and on account of the concentration of this tholeiitic magmatism towards the boundary between the Río de la Plata Craton and the Brasilian mobile belt, Iacumin et al. (2003) emphasized the major role played by upper mantle edge-driven convection geodynamics on its genesis.

7.2.2. Early Ectasian magmatism

An isolated outcrop of gabbros identified in the Martín García Island (MG205) yielded an age of 1392 ± 11 Ma, with inheritance at ca. 2079 Ma. This early Ectasian age was not reported before within the Buenos Aires-Piedra Alta Province. The gabbro is weakly chemically distinct from the two other analyzed gabbros, in that it displays a boninitic signature and is temporally more directly correlated to the granites of the Andean-type Candeias arc (e.g. Santos et al., 2008).

7.2.3. Stenian magmatism

Another gabbro unit that is poorly exposed in the Martín García Island airstrip (MG207), and nearby area (MG202) – was formed during the Stenian at ca. 1193 Ma (MG207). This age was not reported before in the Buenos Aires-Piedra Alta Province. As a first approach, the chemical signature of this unit appears to indicate a magmatic arc. Yet, given the contamination of the mafic magma with Transplatense crust as indicated by the $T_{DM\text{-}Hf}$ 2.00 Ga and ε_{Hf} −0.1, we interpret the chemistry of this Stenian gabbro as inherited from the Transplatense crust (Transplatense arc). In this scenario, we envision the Stenian gabbro actually is a product of extensional magmatism roughly coeval and occurring in a similar geotectonic setting with the Nova Floresta gabbroic sill of 1198 ± 3 Ma (Tohver et al., 2002-Figs. 1 and 3) in the northern part of the Sunsás Belt (Rondônia) and the 1110 Ma old layered gabbros of Rincón del Tigre, eastern Bolivia (Prendergast, 2000-Fig. 1; Teixeira et al., 2015-Fig. 1). Other gabbros in the interior of the Amazon Craton are interpreted as formed during the distal extensional event of the Sunsás Orogen, such as the Cachoeira Seca troctolite of 1186 ± 13 Ma (U-Pb in baddeleyite; Santos et al., 2002-Fig. 7). In this context, the Stenian gabbros of Martín García Island are related to a far-field extensional or transtensional event associated with the Sunsás Orogen. Otherwise, they represent intraplate magmatism pre-dating Rodinia breakup, as suggested by Teixeira et al. (2015) for the coeval Rincón del Tigre layered gabbros of eastern Bolivia. As a first approach, we consider that the extensional/transtensional stress field may account for the amphibolite-facies metamorphism of the Martín García Stenian gabbros.

8. Conclusions

The investigated area is not exclusively Rhyacian in age, but includes Statherian, Ectasian, and Stenian gabbros. The last two correlate to the Sunsás Orogen (Candeias and Sunsás collisional orogenies; Santos et al., 2008) and were emplaced in the craton as a distal effect of the Sunsás collisions from the west.

Magmatic rocks cropping out in the Martín García, Dos Hermanas, and Sola Islands, within the Río de la Plata Craton, have provided a means to interpret the evolution and origin of arc-related Transplatense magmas. Ages obtained for the latter rocks span from ca. 2127 Ma to 2090 Ma (ε_{Hf} data averaging +3.62) indicate their derivation from rather juvenile Neoarchean crust.

Three age groups of mafic rocks are identified: Statherian (1724–1734 Ma), early Ectasian (1392 Ma), and Stenian (1184 Ma) gabbros. It is noteworthy that in spite of their different ages, the Statherian, early Ectasian and Stenian gabbros have similar geochemical signatures (Island Arc Basalts (IAB) primitive mantle signature with enrichment of Large Ion Lithophile Elements (LILE) such as Rb, K, Sr, Ba, and depletion of High Field Strength Elements (HFSE) such as Nb, Th and Ti). These inherited trace element features represent an active mantle during this large range of ages, hence pointing to a similar parent magma. Notably, these geochemical features are identified in other magmatic-arc mantle sources (e.g. Debari, 1994, 1997).

Towards the end of the Transplatense subduction that led to the collision and amalgamation of the proto Río de la Plata Archean fragments into the fully amalgamated Río de la Plata Craton at Rhyacian times (see Fig. 5 in Chernicoff et al., 2014), a slab break-off caused the contamination of the sub-lithospheric mantle. An evidence of this mantle metasomatism is given by the LILE enrichment and HFSE depletion related to the input of slab fluids. It is less likely that such contamination of the sub-lithospheric mantle occurred in Statherian times related with partial melting at the base of the lower crust, because of the lack of alkaline magmatism.

The chemical composition of the granitoids/orthogneisses of the Martín García, Sola, and Dos Hermanas Islands plot in the field of the Transplatense calc-alkaline arc defined by its main exposures in Uruguay and Argentina, and delineate a typical calc-alkaline trend (Fig. 9a).

We consider that cumulate gabbros in the Buenos Aires-Piedra Alta Province (e.g. Villar and Segal, 1990; Bossi et al., 1996), that are part of the early Transplatense magmatism – originated at the subduction stage, i.e. as early as at ca. 2.2 Ga – being representative of the parental magma. Other Transplatense mafic and ultramafic rocks, such as the hornblendites of the Marincho Complex, whose composition is provided by Preciozzi and Bourne (1993), and the Mahoma and Rospide Gabbros (e.g. Bettucci et al., 2010, and references therein), are also representing such primitive parental magma. Their composition is also similar to other primitive magmas of arc settings (cf. Debari, 1994; Fig. 9a).

The Statherian dykes have a primitive magma composition determined by Iacumin et al. (2001). Their composition corresponds to high-Mg, low-Al primitive tholeiite, with similar major-element chemistry to other suggested primary magmas in arc settings (e.g. Debari, 1994) (Fig. 9a).

The occurrence of cumulate gabbros in the Buenos Aires-Piedra Alta Province (e.g. Villar and Segal, 1990; Bossi et al., 1996) as part of the early Transplatense magmatism –originated at the subduction

stage, i.e. as old as 2.2 Ga– is bound to be representative of the parental magma. The chemical signature of such magma remained as a 'fingerprint' up to Stenian times, as shown by the ratio V/(Ti/1000) = 10, the low thorium abundance (e.g., sample MG200: 0.05 ppm, versus 0.065 ppm in the mantle).

Broadly considered, the long lasting primitive magma fingerprint of the magmatic rocks of the Buenos Aires-Piedra Alta Province from early Transplatense subduction through Statherian extensional tectonics, as well as the newly identified Ectasian and Stenian gabbros, points to the existence of magma chambers intermittently active within that lapse with identical composition of their sources (see e.g. Hartmann et al., 2003a,b). Similar examples of long standing primitive magma 'fingerprint' are encountered at other locations and times, e.g. Early Paleozoic Fiambalá magmatic arc gabbroic intrusions (northwestern Argentina; Debari, 1994, 1997), and the Statherian mafic Vespor suite of the Juruena magmatic arc (SW Amazon; Scandolara et al., 2014).

The studied area demonstrates that different tectonic settings are responsible for the evolution of a single parental magma, following either a calc-alkaline (Transplatense-age suite) or a tholeiitic (Statherian magmatism) trend. This is in agreement with the model proposed by Zimmer et al. (2010) who recognized that calc-alkaline and tholeiitic trends are controlled by the content of dissolved water in the magma, this being greater in subduction zones (calc-alkaline magmatism) and lower in extensional settings (tholeiitic magmatism in mid-ocean ridge, ocean island, or back-arc basin settings).

The eastern part of the craton was strongly affected by Brasilian-age collisions and magmatism. The craton was fragmented, deformed by Brasilian-age shear zones, and infiltrated by Neoproterozoic granitoids, forming complex mosaics of pieces of craton and post-craton characterizing a metacratonic configuration following the concept of Liégeois et al. (2013). Other metacratonic areas within the craton are difficult to detect due to extensive cover in the central, southern and western areas of the craton. However, the study area of Martín García and surroundings records the Brasilian-age activity registered in several lower intercept ages.

The word "Trans-Amazon" of Hurley et al. (1967) is used to encompass the dominantly Rhyacian orogen in northern South America and northern Amazon Craton. This is an event inherent to the Amazon Craton and its name applied to other cratons is not adequate. The name "Transplatense" introduced by Santos et al. (2017) is applied to the dominant orogen present in the Río de la Plata Craton, which is comparable in age to the classic Trans-Amazon Orogen of the Amazon Craton.

Acknowledgements

The present investigation forms part of the Project Geochronology of the Río de la Plata Craton, being carried out by the Geological and Mining Survey of Argentina (SEGEMAR). Part of the data was produced under support of CNPQ (Conselho Nacional de Pesquisa e Desenvolvimento Tecnológico) of Brazil to the senior author (scholarship 229433/2013-8). Zircon grains were analyzed on the SHRIMP II operated by a Western Australia university-government consortium. BSE (Back-Scattered Electrons) images were carried out using facilities at the CMCA (Centre for Microscopy, Characterization, and Analyses), which is supported by funding from UWA and the governments of Western Australia and Australia.

References

Almeida, F.F.M., Hasui, Y., Neves, B.B.B., 1976. The Upper Precambrian of South America, vol. 7. Boletim de Geociências, Universidade de São Paulo, pp. 45–80.

Angeletti, M., Chichorro, M., Frisicale, M.C., Castro, A., Dimieri, L.V., 2014. Nuevas edades radiométricas U-Pb SHRIMP en Tandilia, Cerro Siempre Amigos, Sierras de Azul, Buenos Aires, Argentina. In: Congreso Geológico Argentino, 19th, Córdoba, Argentina, Abstracts T8–1.

Bettucci, L.S., Peel, E., Oyhantçabal, P., 2010. Precambrian geotectonic units of the Río de la Plata Craton. Int. Geol. Rev. 52 (1), 32–50.

Biermanns, L., 1996. Chemical classification of gabbroic-dioritic rocks based on TiO_2, SiO_2, FeO_{TOT}, MgO, K_2O, Y, and Zr. In: International Symposium on Andean Geology (ISAG), 3rd, St. Malo, France, pp. 547–550.

Blichert-Toft, J., Albarède, F., 1997. The Lu-Hf isotope geochemistry of chondrites and the evolution of the mantle-crust system. Earth Planet. Sci. Lett. 27, 243–258.

Bossi, J., Campal, N., 1992. Magmatismo y tectónica transcurrente durante el Paleozoico Inferior en Uruguay. In: Gutierrez- Marco, J.G., Saavedra, J., Rabano, I. (Eds.), Paleozoico Inferior de Iberoamérica. Universidad de Extremadura, Mérida, pp. 343–356.

Bossi, J., Cingolani, C., 2009. Extension and general evolution of the Río de la Plata Craton. In: Gaucher, C., Sial, A.N., Halverson, G.P., Frimmel, H.E. (Eds.), Neoproterozoic-cambrian Tectonics, Global Change and Evolution: a Focus on Southwestern Gondwana, vol. 16. Developments in Precambrian Geology, pp. 73–85.

Bossi, J., Ferrando, L., 2001. Carta Geológica del Uruguay, versión 2.0. Escala 1: 500000. Geoeditores. Montevideo, Uruguay.

Bossi, J., Mutti, D., Piñeyro, D., Di Marco, A., 1996. El cinturón arqueano uruguayo de San José: caracterización litogeoquímica de su área tipo. In: Congreso Geológico Argentino, 13rd ands Congreso de Exploración de Hidrocarburos, vol. 3. Actas, pp. 567–579, 3rd.

Bossi, J., Ferrando, L., Montaña, J., Campal, N., Morales, H., Gancio, F., Schipilov, A., Piñeyro, D., Sprechmann, P., 1998. Carta Geológica del Uruguay, Escala 1: 500.000. Digital Versión 1.0. Geoeditores-Facultad de Agronomía, Montevideo.

Camozzatto, E., Philipp, R.P., Chemale Jr., F., 2013. Idades Estaterianas no Domo da Vigia: complexos Vigia e Porongos, Metagranito Seival e Anfibolito Tupi Silveira, Bagé, RS. In: International Symposium on Tectonics, 8th, Simpósio Nacional de Estudos Tectônicos, 14th, 2013, Chapada dos Guimarães. Cuiabá: SBG-MT, vol. 1. CD-ROM.

Chemale Jr., F., Phillip, R.P., Dussin, I.A., Formoso, M.L.L., Kawashita, K., Bertotti, A.L., 2011. Lu-Hf and U-Pb age determination of Capivarita anorthosite in the Dom Feliciano belt, Brazil. Precambrian Res. 186, 117–126.

Chernicoff, C.J., Zappettini, E.O., Peroni, J., 2014. The Rhyacian El Cortijo suture zone: aeromagnetic signature and insights for the geodynamic evolution of the southwestern Río de la Plata Craton, Argentina. Geosci. Front. 5, 43–52.

Chernicoff, C.J., Pereyra, F., Santos, Zappettini, E.O., 2015. Primeras edades U-Pb SHRIMP del craton Río de la Plata en el subsuelo del área metropolitan de Buenos Aires. Rev. la Asoc. Geol. Argent. Nota Breve 72 (4), 575–577.

Chernicoff, C.J., Zappettini, E.O., Santos, J.O.S., Pesce, A., McNaughton, N.J., 2016. Zircon and titanite U-Pb SHRIMP dating of unexposed basement units of the Buenos Aires region, southeastern Río de la Plata Craton, Argentina. Int. Geol. Rev. 58 (5), 643–652.

Cingolani, C.A., 2011. The Tandilia System of Argentina as a southern extension of the Río de la Plata Craton: an overview. Int. J. Earth Sci. 100 (2), 221–242.

Cingolani, C.A., Hartmann, L.A., Santos, J.O.S., McNaughton, N.J., 2002. U–Pb SHRIMP dating of zircons from the Buenos Aires complex of the Tandilia belt, Río de la Plata Craton, Argentina. In: Proceedings 15 Congreso Geológico Argentino (El Calafate, Santa Cruz), vol. 1. Actas, pp. 149–154.

Cingolani, C.A., Santos, J.O.S., McNaughton, N.J., Hartmann, L.A., 2005. Geocronología U-Pb SHRIMP sobre circones del Granitoide Montecristo. Tandil, Provincia de Buenos Aires, Argentina. In: Congreso Geológico Argentino, 16th, La Plata 1, Proceedings, pp. 299–302.

Cingolani, C.A., Santos, J.O.S., Griffin, W., 2010. New insights of the Paleoproterozoic basement of Tandilia belt, Río de la Plata Craton, Argentina: first Hf isotope studies on zircon crystals. In: Symposium GEOSUR, Extended Abstract, Mar del Plata, Argentina, pp. 21–24.

Dalla Salda, L., 1981. El basamento de la Isla Martín García, Río de la Plata. Rev. la Asoc. Geol. Argent. 36 (1), 29–43.

Debari, S.M., 1994. Petrogenesis of the Fiambalá gabbroic intrusion, northwestern Argentina, a deep crustal syntectonic pluton in a continental magmatic arc. J. Petrol. 35 (3), 679–713.

Debari, S.M., 1997. Evolution of magmas in continental and oceanic arcs: the role of the lower crust. Can. Mineralogist 35, 501–519.

Dragone, G.N., Ussami, N., Gimenez, M.E., Klinger, F.G.L., Chaves, C.A.M., 2017. Western Paraná suture/shear zone and the limits of Rio Apa, Rio Tebicuary and Rio de la Plata cratons from gravity data. Precambrian Res. 291, 162–177.

Ernst, R.E., 2014. Large Igneous Provinces. Cambridge University Press, ISBN 978-0-521-87177-8.

Fernandes, L.A.D., Koester, E., 1999. The Neoproterozoic Dorsal de Canguçu strike-slip shear zone: its nature and role in the tectonic evolution of southern Brazil. J. Afr. Earth Sci. 29, 3–24.

Fuck, R.A., Neves, B.B.B., Schobbenhaus, C., 2008. Rodinia descendants in south America. Precambrian Res. 160, 108–126.

Fulfaro, V.J., 1996. Geología del Paraguay oriental. In: Comin-Chiaramonti, P., Gomes, C.B. (Eds.), Alkaline Magmatism in Central-eastern Paraguay. Edusp/Fapesp, São Paulo, pp. 17–29.

Gaucher, C., Bossi, J., Blanco, G., 2009. Palaeogeography. Neoproterozoic-Cambrian evolution of the Río de la Plata Palaeocontinent. In: Gaucher, C., Sial, A.N., Halverson, G.P., Frimmel, H.E. (Eds.), Neoproterozoic-cambrian Tectonics, Global Change and Evolution: a Focus on Southwestern Gondwana, vol. 16.

Developments in Precambrian Geology, pp. 131–141.
Gaucher, C., Frei, R., Chemale Jr., F., Frei, D., Bossi, J., Martínez, G., Chiglino, L., Cernuschi, F., 2011. Mesoproterozoic evolution of the Río de la Plata Craton in Uruguay: at the heart of Rodinia? Int. J. Earth Sci. 100 (2), 273–288.
Gill, J.B., 1981. Orogenic Andesites and Plate Tectonics. Springer-Verlag, 358 pp.
Griffin, W.L., Pearson, N.J., Belousova, E.A., Jackson, S.R., van Achterbergh, E., O'Reilly, S.Y., Shee, S.R., 2000. The Hf isotope composition of cratonic mantle: LAM-MC-ICPMS analysis of zircon megacrysts in kimberlites. Geochim. Cosmochim. Acta 64, 133–147.
Griffin, W.L., Belousova, E.A., Shee, S.R., Pearson, N.J., O'Reilly, S.Y., 2004. Archean crustal evolution in the northern Yilgarn Craton: U–Pb and Hf-isotope evidence from detrital zircons. Precambrian Res. 131, 231–282.
Halls, H.C., Campal, N., Davis, D.W., Bossi, J., 2001. Magnetic studies and U–Pb geochronology of the Uruguayan dike swarm, Río de la Plata Craton, Uruguay: paleomagnetic and economic implications. J. S. Am. Earth Sci. 14, 349–361.
Hartmann, L.A., Piñeyro, D., Bossi, J., Leite, J.A.D., McNaughton, N.J., 2000. Zircon U-Pb SHRIMP dating of Paleoproterozoic Isla Mala granitic magmatism in the Río de la Plata Craton, Uruguay. J. S. Am. Earth Sci. 13, 105–113.
Hartmann, L.A., Campal, N., Santos, J.O.S., McNaughton, N.J., Bossi, J., Schipilov, A., 2001. Archean crust in the Río de la Plata Craton, Uruguay—SHRIMP U–Pb reconnaissance geochronology. J. S. Am. Earth Sci. 14, 557–570.
Hartmann, L.A., Santos, J.O.S., Cingolani, C.A., McNaughton, N.J., 2002. Two palaeoproterozoic orogenies in the evolution of the Tandilia belt, Buenos Aires, as evidenced by zircon U–Pb SHRIMP geochronology. Int. Geol. Rev. 44, 528–543.
Hartmann, L.A., Bitencourt, M.A., Santos, J.O.S., McNaughton, N.J., Rivera, C., Betiollo, L., 2003a. Prolonged paleoproterozoic magmatic participation in the neoproterozoic Dom Feliciano belt, Santa Catarina, Brazil, based on zircon U–Pb SHRIMP geochronology. J. S. Am. Earth Sci. 16, 477–492.
Hartmann, L.A., Santos, J.O.S., Leite, J.A.D., Porcher, C., McNaughton, N.J., 2003b. Metamorphic evolution and U-Pb zircon SHRIMP geochronology of the Belizário ultramafic amphibolite, Encantadas Complex, southernmost Brazil. An. Acad. Bras. Ciências 75 (3), 393–403.
Hartmann, L.A., Chemale Jr., F., Philipp, R.P., 2007. Evolução Geotectônica do Rio Grande do Sul no Pré- Cambriano. In: Ianuzzi, R., Frantz, J.C. (Eds.), 50 anos de Geologia no Rio Grande do Sul, Editora Comunicação e Identidade, 1ª ed., vol. 1. Instituto de Geociências. Contribuições, Porto Alegre, pp. 97–123. CIGO. IG-UFRGS.
Hartmann, L.A., Bossi, J., Santos, J.O.S., Mc Naughton, N.J., Piñeyro, D., 2008a. Geocronología SHRIMP U-Pb en circones del Gabro Rospide del Cinturón Paleoproterozoico San José, Terreno Piedra Alta, Uruguay: una prueba geocronológica de magmas coetáneos. Rev. Soc. Urug. Geol. 15, 40–45.
Hartmann, L.A., Liu, D., Wang, Y., Massonne, H.J., Santos, J.O.S., 2008b. Protolith age of Santa Maria Chico granulites dated on zircons from an associated amphibolite-facies granodiorite in southernmost Brazil. An. Acad. Bras. Ciências 80 (3), 1–9.
Hartmann, L.A., Philipp, R.P., Santos, J.O.S., McNaughton, N.J., 2011. Time frame of the 753–680 Ma juvenile accretion during the São Gabriel orogeny, Southern Brazilian shield. Gondwana Res. 19, 84–99.
Hawkesworth, C.J., Kemp, A.I.S., 2006. Using hafnium and oxygen isotopes in zircons to unravel the record of crustal evolution. Chem. Geol. 226, 144–162.
Heaman, L.M., 2009. The application of U–Pb geochronology to mafic, ultramafic and alkaline rocks: an evaluation of three mineral standards. Chem. Geol. 261, 42–51.
Hurley, P.M., Almeida, F.F.M., Melcher, G.C., Cordani, U.G., Rand, J.R., Kawashita, K., Vandoros, P., Pinson Jr., W.H., Fairbairn, H.W., 1967. Test of continental drift by comparison of radiometric ages. Sci. New Ser. 157 (3788), 495–500.
Iacumin, M., Piccirillo, E.M., Girardi, V.A.V., Teixeira, W., Bellieni, G., Echeveste, H., Fernandez, R., Pinese, J.P.P., Ribot, A., 2001. Early Proterozoic calc-alkaline and Middle Proterozoic tholeiitic dyke swarms from central-eastern Argentina: petrology, geochemistry, Sr-Nd isotopes and tectonic implications. J. Petrol. 42 (11), 2109–2143.
Iacumin, M., De Min, A., Piccirillo, E.M., Bellieni, G., 2003. Source mantle heterogeneity and its role in the genesis of late archaean-proterozoic (2.7-1.0 Ga) and mesozoic (200 and 130 Ma) tholeiitic magmatism in the south american platform. Earth Sci. Rev. 62, 365–397.
Lena, L.O.F., Pimentel, M.M., Philipp, R.P., Armstrong, R., Sato, K., 2014. The evolution of the Neoproterozoic São Gabriel juvenile terrane, southern Brazil based on high spatial resolution U-Pb ages and $\delta^{18}O$ data from detrital zircons. Precambrian Res. 247, 126–138.
Liégeois, J.P., Abdelsalam, M.G., Ennih, N., Ouaba, A., 2013. Metacraton: Nature, genesis and behavior. Gondwana Res. 23 (1), 220–237.
Ludwig, K.R., 2003. Isoplot 3.00, a Geochronological Took-kit for Excel, vol. 4. Berkely Geochronology Center Special Publication, 67 pp.
Ludwig, K.R., 2009. SQUID 2: a User's Manual, Rev. 2.50, 12 Apr, 2009, vol. 5. Berkeley Geochronology Centre Special Publication, 110 pp.
Maniar, P.D., Piccoli, P.M., 1989. Tectonic discrimination of granitoids. Geol. Soc. Am. Bull. 101, 635–643.
Martínez, J.C., Dristas, J.A., Van Den Kerkhof, A.M., Wemmer, K., Massonne, H.J., Theye, T., Frisicale, M.C., 2013. Late-Neoproterozoic hydrothermal fluid activity in the Tandilia belt, Argentina. Rev. la Asoc. Geol. Argent. 70 (3), 410–426.
Mattinson, J.M., Graubard, C.M., Parkinson, D.L., McClelland, W.C., 2013. U-Pb reverse discordance in zircons: the role of fine-scale oscillatory zoning and submicron transport of Pb. In: Basu, A., Hart, S. (Eds.), Earth Processes: Reading the Isotopic Code. Geophysical Monograph Series, American Geophysical Union. https://doi.org/10.1029/GM095.
Mazzucchelli, M., Rivalenti, G., Piccirillo, E.M., 1995. Petrology of the Proterozoic mafic dyke swarms of Uruguay and constraints on their mantle source composition. Precambrian Res. 74, 177–194.
Neves, B.B.B., Fuck, R.A., Pimentel, M.M., 2014. The Brasiliano collage in South America: a review. Braz. J. Geol. 44 (3), 493–518.
Oriolo, S., Oyhantçabal, P., Wemmer, K., Basei, M.A.S., Benowitz, J., Pfänder, J., Hannich, F., Siegesmund, S., 2016. Timing of deformation in the Sarandí del Yí Shear Zone, Uruguay: implications for the amalgamation of western Gondwana during the Neoproterozoic Brasiliano-Pan-African Orogeny. Tectonics 35, 754–771. https://doi.org/10.1002/2015TC004052.
Oyhantçabal, P., Siegesmund, S., Wemmer, K., 2011. The Río de la Plata Craton: a review of units, boundaries, ages and isotopic signature. Int. J. Earth Sci. 100, 201–220.
Pankhurst, R.J., Ramos, V.A., Linares, E., 2003. Antiquity of the Río de la Plata Craton in Tandilia, southern Buenos Aires Province, Argentina. J. S. Am. Earth Sci. 16, 5–13.
Peel, E., Preciozzi, F., 2006. Geochronologic synthesis of the Piedra Alta terrane, Uruguay. In: South American Symposium on Isotope Geology, pp. 234–237, 5th, Punta del Este, Uruguay.
Preciozzi, F., Bourne, J.H., 1993. Geochemistry and geochronology of three plutons from Central Uruguay: Tectonic implications for the Transamazonic Orogeny. Rev. Bras. Geociências 24, 167–193.
Prendergast, M.D., 2000. Layering and precious metal mineralization in the Rincón del Tigre complex, eastern Bolivia. Econ. Geol. 95 (1), 113–130.
Ramos, V.A., Vujovich, G., Martíno, R., Otamendi, J., 2010. Pampia: a large cratonic block missing in the Rodinia supercontinent. J. Geodyn. 50, 243–255.
Rapela, C.W., Pankhurst, R.J., Casquet, C., Fanning, C.M., Baldo, E.G., González-Casado, J.M., Galindo, C., Dahlquist, J., 2007. The Río de la Plata Craton and the assembly of SW Gondwana. Earth Sci. Rev. 83, 49–82.
Rapela, C.W., Fanning, C.M., Casquet, C., Pankhurst, R.J., Spalletti, L., Poiré, D., Baldo, E.G., 2011. The Río de la Plata craton and the adjoining Pan-African/Brasiliano terranes: their origins and incorporation into south-west Gondwana. Gondwana Res. 20 (4), 673–690.
Ribot, A., Cingolani, C.A., Piñeyro, D., Bossi, J., Basei, M., Uriz, N., 2013. Milonitas graníticas de la isla San Gabriel, Uruguay: cinemática de la deformación y geocronología U-Pb. In: 1 Simposio de Minería y desarrollo del Cono Sur, Congreso Uruguayo de Geología, 7th, Montevideo.
Santos, J.O.S., 2016. The Mesoproterozoic belts of South America. In: Brazilian Geological Congress, 48th, Porto Alegre, Brazil. Thematic session 10, paper 7094, Archean and Proterozoic Terranes.
Santos, J.O.S., Hartmann, L.A., McNaughton, N.J., Fletcher, I.R., 2002. Timing of mafic magmatism in the Tapajós Province (Brazil) and implications for the evolution of the Amazon Craton - evidence from baddeleyite and zircon U-Pb SHRIMP geochronology. J. S. Am. Earth Sci. 15, 409–429.
Santos, J.O.S., Hartmann, L.A., Bossi, J., Campal, N., Schipilov, A., Piñeiro, McNaughton, N.J., 2003. Duration of the Trans-Amazonian Cycle and its correlation within South America based on U–Pb SHRIMP geochronology of the la Plata craton, Uruguay. Int. Geol. Rev. 45, 27–48.
Santos, J.O.S., Rizzotto, G.J., Potter, P.E., McNaughton, N.J., Matos, R.S., Hartmann, L.A., Chemale Jr., F., Quadros, M.E.S., 2008. Age and autochthonous evolution of the Sunsás orogen in west Amazon craton based on mapping and U–Pb geochronology. Precambrian Res. 165, 120–152.
Santos, J.O.S., Chernicoff, C.J., Zappettini, E.O., McNaughton, N.J., Hartmann, L.A., 2017. Geographic and temporal extensions of the Río de la Plata Craton, South America and its metacratonic eastern margin (Submitted to International Geology Review).
Scandolara, J.E., Ribeiro, P.S.E., Frasca, A.S.A., Fuck, R.A., 2014. Geochemistry and geochronology of mafic rocks from the Vespor suite in the Juruena arc, Roosevelt-Juruena terrain, Brazil: implications for Proterozoic crustal growth and geodynamic setting of the SW Amazonian craton. J. S. Am. Earth Sci. 53, 20–49.
Scherer, E., Münker, C., Metzger, K., 2001. Calibrating the Lu-Hf clock. Science 293, 683–686.
Schmitt, R.S., Trouw, R.A.J., Van Schmus, W.R., Pimentel, M.M., 2004. Late amalgamation in the central part of West Gondwana: new geochronological data and the characterization of a Cambrian collisional orogeny in the Ribeira Belt (SE Brazil). Precambrian Res. 133, 29–61.
Schobbenhaus, C., Neves, B.B.B., 2003. Geologia do Brasil no contexto da Plataforma Sul-Americana. In: Bizzi, L., Schobbenhaus, C., Vidotti, M.R., Gonçalves, J.H. (Eds.), Geologia, tectônica e recursos minerais do Brasil, Brasília: Serviço Geológico do Brasil-CPRM, pp. 5–54.
Servicio Geográfico Militar del Uruguay, 1996. Ajuste de la red gravimétrica nacional de Uruguay. http://www.sgm.gub.uy/index.php/documentos/cat_view/1-articulos-tecnicos/docdownload/24-ajuste-de-la-red-gravimetrica-nacional.
Siga Júnior, O., Basei, M.A.S., Passarelli, C.R., Harara, O.M., Sato, K., Cury, L.F., Prazeres Filho, H.C., 2007. Geocronologia de rochas gnáissico-migmatíticas e sienograníticas do Núcleo Setuva (PR): implicações tectônicas. Rev. Bras. Geociências 37 (1), 114–128.
Stern, R.A., 2001. A New Isotopic and Trace-element Standard for the Ion Microprobe: Preliminary Thermal Ionization Mass Spectrometry (TIMS) U-Pb and Electron-microprobe Data; Radiogenic Age and Isotopic Studies: Report 14. Geological Survey of Canada, Current Research, ISBN 0-662-30756-9, 2001–F1, 11 pp.
Sun, S.S., McDonough, W.F., 1989. Chemical and isotopic systematics of oceanic basalts; implications for mantle composition and processes. In: Saunders, A.D.,

Norry, M.J. (Eds.), Magmatism in the Ocean Basins, vol. 42. Geological Society of London, London, pp. 313–345.
Teixeira, W., Pinese, J.P.P., Iacumin, M., Girardi, V.A.V., Piccirillo, E.M., Echevest, E.H., Ribot, A., Fernandez, R., Renne, P.R., Heaman, L.M., 2002. Calc-alkaline and tholeitic dike swarms of Tandilia, Río de la Plata Craton, Argentina: U-Pb, Sm-Nd, Rb-Sr, and 40Ar/39Ar data provide new clues for intraplate rifting shortly after the Trans-Amazonian orogeny. Precambrian Res. 119, 329–353.
Teixeira, W., Hamilton, M.A., Lima, G.A., Ruiz, A.S., Matos, R., Ernst, R.E., 2015. Precise ID-TIMS U-Pb baddeleyite ages (1110-1112 Ma) for the Rincón del Tigre-Huanchaca large igneous province (LIP) of the Amazonian Craton: implications for the Rodinia supercontinent. Precambrian Res. 265, 273–285.
Thompson, R.N., 1982. British Tertiary volcanic province. Scott. J. Geol. 18, 49–107.
Tohver, E., van der Pluijm, B.A., van der Voo, R., Rizzotto, G.J., Scandolara, J.E., 2002. Paleogeography of the Amazon craton at 1.2 Ga: early Grenvillian collision with the Llano segment of Laurentia. Earth Planet. Sci. Lett. 199, 185–200.
Villar, M.L., Segal, S.J., 1990. Caracterización petrológica y metalogenética del complejo gábrico próximo a San José de Mayo, Dpto. de San José, Uruguay, Congreso Geológico Uruguayo. Actas, pp. 199–204, 1st.
Whalen, J.B., Currie, K.L., Chappell, B.W., April 1987. A-type granites: geochemical characteristics, discrimination and petrogenesis. Contrib. Mineral. Petrol. 95 (4), 407–419.
Williams, I.S., Hergt, J.M., 2000. U-Pb dating of Tasmanian dolerites: a cautionary tale of SHRIMP analysis of High-U zircon. In: Woodhead, J.D., Hergt, J.M., Noble, W.P. (Eds.), Beyond 2000: New Frontiers in Isotope Geoscience, pp. 185–188. Lorne, 2000. Abstract Proceedings.
Williams, I.S., Compston, W., Black, L.P., Ireland, T.R., Foster, J.J., 1984. Unsupported radiogenic Pb in zircon: a cause of anomalously high Pb-Pb, U-Pb, and Th-Pb ages. Contrib. Mineral. Petrol. 88, 322–327.
Woodhead, J.D., Hergt, J.M., 2005. A preliminary appraisal of seven natural zircon reference materials for *in situ* Hf isotope determination. Geostand. Geoanal. Res. 29 (2), 183–195.
Zimmer, M.M., Plank, T., Hauri, E.H., Yogodzinski, G.M., Stelling, P., Larsen, J., Singer, B., Jicha, B., Mandeville, C., Nye, C.J., 2010. The role of water in generating the calc-alkaline trend: new Volatile data for Aleutian Magmas and a new Tholeiitic index. J. Petrol. 51 (12), 2411–2444.